Journal of Translational Medicine

RESEARCH

Open Access

Adipose-derived stem cell exosomal miR-21-5p enhances angiogenesis in endothelial progenitor cells to promote bone repair via the NOTCH1/DLL4/VEGFA signaling pathway

Le Cao[1†], Kai Sun[1†], Ran Zeng[2] and Haitao Yang[1*]

Abstract

Background Angiogenesis is essential for repairing critical-sized bone defects. Although adipose-derived stem cell (ADSC)-derived exosomes have been shown to enhance the angiogenesis of endothelial progenitor cells (EPCs), the underlying mechanisms remain unclear. This study aims to explore the effects and mechanisms of ADSC-derived exosomes in enhancing bone repair by promoting EPC angiogenesis.

Methods Transmission electron microscopy, nanoparticle tracking analysis, and DiI reagent kit were employed to identify ADSC-derived exosomes and their internalization by EPCs. Micro-CT analysis, H&E staining, and Masson staining were used to assess bone mineral density (BMD), bone volume fraction (BV/TV), trabecular thickness (Tb.Th), and trabecular number (Tb.N), as well as the pathological changes and fibrosis at defect sites. Cell viability, migration, invasion, and tube formation of EPCs were evaluated using CCK-8, wound healing, Transwell, and tube formation assays. Immunohistochemical staining, RT-PCR, and Western blotting were utilized to measure the gene and protein expression of markers such as CD31, VEGFA, OCN, RUNX2, NOTCH1, and DLL4. Gene sequencing and bioinformatics analyses were conducted to identify the most highly expressed miRNA in exosomes, while miRDB and dual-luciferase reporter assays were used to explore the interaction between miR-21-5p and NOTCH1.

Results The ADSC-derived exosomes, averaging 126 nm in diameter, were internalized by EPCs. In vivo, these exosomes promoted new bone formation, increased BMD, BV/TV, Tb.Th, and Tb.N, reduced pathological damage to cranial defect tissues, enhanced vascular and bone tissue regeneration, and upregulated OCN and RUNX2 expression. In vitro, ADSC-derived exosomes enhanced EPC viability, migration, invasion, and tube formation. Both in vivo and in vitro experiments demonstrated that ADSC-derived exosomes upregulated CD31 and VEGFA expression. miR-21-5p, the most highly expressed miRNA in ADSC-derived exosomes, was found to target NOTCH1. Overexpression of miR-21-5p in these exosomes facilitated EPC migration, tube formation, and VEGFA expression while downregulating NOTCH1 and DLL4 expression. Inhibition of miR-21-5p produced opposite effects on EPCs.

[†]Le Cao and Kai Sun have contributed equally to this work.

*Correspondence:
Haitao Yang
yang56863789@163.com
Full list of author information is available at the end of the article

Conclusions These findings indicate that miR-21-5p in ADSC-derived exosomes promotes angiogenesis in EPCs to accelerate bone repair by targeting the NOTCH1/DLL4/VEGFA signaling pathway, offering a potential therapeutic strategy for bone defect treatment.

Keywords Exosomes, Angiogenesis, Bone repair, Adipose-derived stem cells, Endothelial progenitor cells

Graphical Abstract

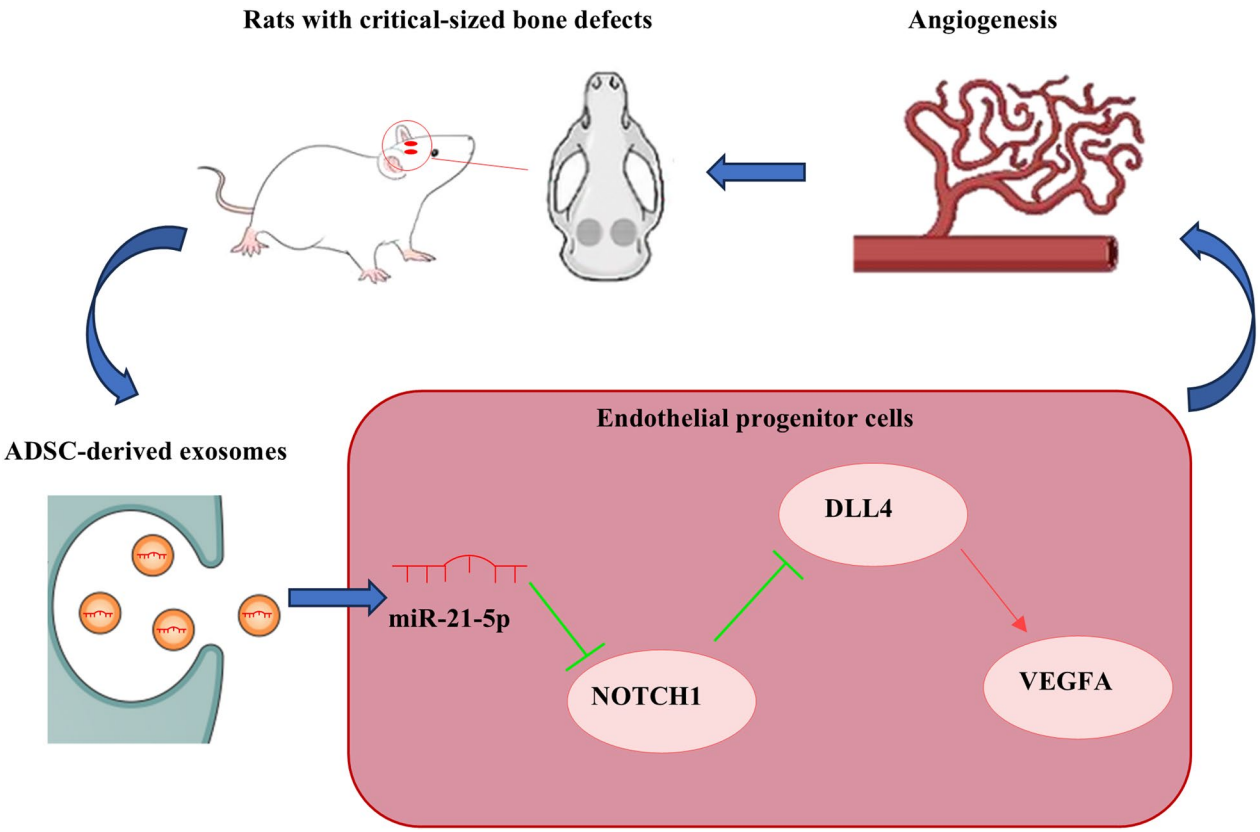

Introduction

It is widely known that critical-sized bone defects (CSBDs) refer to bone defects that are unable to spontaneously heal without intervention, which extremely affects the quality of life of patients [1]. The successful repair of CSBDs caused by trauma, tumor, infection, and congenital malformation is still one of the existing thorny conundrums in bone tissue engineering [2]. Although traditional therapeutic methods have already made tremendous progress in the clinical treatment of CSBDs, there are still some blemishes of them. For instance, autogenous bone grafts may cause a dilemma for their clinical application due to secondary trauma generated by reoperation, and allogeneic bone grafts usually possess a worse biological activity owing to immunological rejection [3, 4]. In addition, there are some other intractable issues for the clinical application of both autogenous bone grafts and allogeneic bone grafts, such as the low survival of transplanted cells, the low migration velocity of new bone tissue from the periphery to the center of the scaffold, and the inhibition of the osteogenic differentiation of cells [5, 6]. Angiogenesis plays an essential role in maintaining sufficient blood supply in the progression of the repair of CSBDs, especially for the stage of the formation of primitive callus. It was reported that the deficiency of vascularization in the implanted bone tissue is one of the leading factors to induce the inadequate nutrition of bone tissue, thereby reducing the formation of regenerated bone and limiting the repair of CSBDs [7, 8]. The neovascularization is responsible for transporting oxygen, nutrients, various cell types, and cytokines to the damaged site to promote the repair of CSBDs [9].

Meanwhile, it has been discovered that osteocytes and osteoprogenitor cells tend to accumulate near vascular endothelial cells at the site of new bone formation, indicating that angiogenesis is also interdependent with osteogenesis [10]. Therefore, it is extensively studied and accepted that the importance of the regulation of angiogenesis at bone defect sites in facilitating the repair of CSBDs.

Adipose-derived stem cells (ADSCs), one kind of cells extracted from adipose tissue with high proliferation and multipotent differentiation potential, not only possess the potential to differentiate into endothelial cells but also promote the formation of new blood vessels by secreting vascular endothelial growth factor and exosomes [11, 12]. Although the direct transplantation of ADSCs has been shown to promote angiogenesis in ischemic areas, the transplanted ADSCs also face some issues, such as low survival rate, short residence time, and immune rejection [13, 14]. The exosomes secreted by cells are important mediators for intercellular information transmission, whose inside contains lipids, nucleic acids, and proteins [15]. The nucleic acids, such as messenger RNAs (mRNAs) and micro RNAs (miRNAs), contained in exosomes are internalized by receptor cells to regulate gene expression and cellular behavior [16]. Meanwhile, it has been indicated that the transplantation of exosomes secreted by stem cells not only possesses the same promoting effect on vascular production but also effectively avoids triggering immune rejection reactions with the host compared with transplanted stem cells [17, 18]. Although ADSC-derived exosomes have been proven to promote endothelial injury repair and angiogenesis, the related mechanisms are still unclear [19]. Therefore, cell-free therapy based on exosomes, the preferred strategy for promoting angiogenesis, is gradually becoming a research hotspot. Endothelial progenitor cells (EPCs), the precursor cells of vascular endothelial cells, not only promote angiogenesis by secreting angiogenic growth factors but also integrate themselves into newly developed capillaries to stimulate angiogenesis [20]. Out of the promotional ability of EPCs to angiogenesis, their application scope in various orthopedic diseases is continuously expanding, especially in areas particularly susceptible to the blood supply, such as CSBDs, fractured tissue, transplanted tissue, and ischemic limbs [21, 22]. Although previous studies have indicated that the co-cultivation between ADSCs and EPCs contributes to promoting the proliferation, migration, and vasoactivity of EPCs, the dominant regulated factors and pathways for effects exerted by ADSCs are still unclear [23].

Due to the crucial role of angiogenesis in CSBDs, this study aims to investigate whether ADSC-derived exosomes promote angiogenesis to repair cranial defects in vivo and the effects of ADSC-derived exosomes on EPCs in vitro. Meanwhile, this paper also explores the essential role of miR-21-5p in ADSC-derived exosomes in affecting EPCs.

Materials and methods

Materials and reagents

The primary basic culture mediums of rat ADSCs and EPCs were purchased from iCell Bioscience (Shanghai, China). The 10% FBS without exosomes was obtained from BioMed Biotech (Wuhan, China). The exosome extraction kit was bought from KeyGen Biotech (Nanjing, China). The H&E staining kit, Masson staining kit, and crystal violet staining solution were purchased from Beyotime (Shanghai, China). The Lipofectamine 2000 reagent was provided by ThermoFisher Scientific (MA, USA). The cell counting kit-8 (CCK-8) was bought from Dojindo Laboratories (Kyushu Island, Japan). The Dil reagent kit was provided by Umibio (Shanghai, China). The Matrigel was purchased from BD Biosciences (California, USA). The Trizol reagent and the BCA kit were bought from Biosharp (Toronto, Canada). The reverse transcription kit and the QPCR reaction kit were obtained from YeShen Biotech (Shanghai, China). The GenSeq® Small RNA Library Prep Kit was purchased from GenSeq (Stockholm, Sweden). The primary antibodies of CD9 and CD63 (the exosomal markers), platelet/endothelial cell adhesion molecule 1 (CD31), osteocalcin (OCN), runt-related transcription factor 2 (RUNX2), and anti-vascular endothelial growth factor A (VEGFA), anti-neurogenic locus notch homolog protein 1 (NOTCH1), and anti-Delta-like 4 (DLL4) were obtained from BIOSS (Beijing, China), but the primary antibody of β-actin was provided by Serivicebio (Wuhan, China).

Cell culture

The rat ADSCs and EPCs were purchased from iCell Bioscience Inc. (Shanghai, China), among which ADSCs were employed for the extraction of exosomes, and EPCs were adopted for the subsequent studies. ADSCs and EPCs were cultured in the corresponding primary basic culture medium supplemented with 10% FBS without exosomes at 37℃ and 5% CO_2, respectively. The culture medium of ADSCs and EPCs was replaced every two days until their coverage achieved 80%. According to the previous study, in the present study, EPCs and ADSCs were respectively seeded in the lower chamber and upper chamber of Transwell with a proportion of 2:1 for 48 h to establish the co-cultivation system between EPCs and ADSCs [24]. The co-cultivation system between EPCs and ADSC-derived exosomes was created by directly adding exosomes into EPCs.

Extraction and identification of exosomes

The ADSC-derived exosomes were extracted in the light of the previous study [25]. After the exosomes in the supernatant of ADSCs were successfully extracted with the help of an exosome extraction kit, the transmission electron microscope (TEM) and nanoparticle tracking analysis (NTA) technology were respectively applied to observe and determine the size and concentration of exosomes and the Western blot approach was used to determine the characteristic proteins of exosomes, including CD9 and CD63.

Exosome internalization assay

In the present study, the Dil reagent kit was adopted to finish the exosome internalization assay. In short, after the ADSC-derived exosomes were successfully stained by 1 μM Dil dyeing working solution, the Dil-stained exosomes were co-cultured with EPCs for 48 h. Then, all EPCs were fixed with polyformaldehyde and counterstained by DAPI solution. Finally, the EPCs were visualized by a fluorescence microscope to determine the number of internalized exosomes.

Gene sequencing of exosomes and bioinformatics analysis

After the miRNAs in ADSC-derived exosomes were extracted and the miRNA library of exosomes was constructed using GenSeq® Small RNA Library Prep Kit according to the producer's instructions, the miRNA products within the length range were selected through fragment screening. The gene sequencing was performed on the Illumina HiSeq sequencer (California, USA). The Venn diagram among the miRanda (http://www.microrna.org/microrna/getDownloads.do), RNAhybird (https://bibiserv.cebitec.uni-bielefeld.de/rnahybrid), Targetscan (http://www.targetscan.org/vert_80/), and the gene sequencing results was constructed to screen the highest expressed miRNA in ADSC-derived exosomes.

Animals and cranial deficiency model

All 30 seven-week-age SD male rats (260–280 g) brought from SiPeiFu Biotechnology (Beijing, China) were randomly divided into six cages and were adaptively fed in the Animal Experiment Center of Fuyang Hospital Affiliated to Anhui Medical University for two weeks. The Ethics Committee of Fuyang Hospital Affiliated to Anhui Medical University proved all animal experimental procedures with the ethical code, MDL2022-12–27-01. We made efforts to minimize the number of animals utilized and to decrease their suffering. The location of animals and cages was unchanged until all experiments were finished to minimize potential confounders. The cranial deficiency model was successfully established in line with the previous study [26]. After rats were anesthetized by sodium pentobarbital (40 mg/kg) via intraperitoneal injection and sterilized with iodophor in their forehead skin, a sagittal incision with a diameter of about 2 cm was conducted above the forehead. After the skin and skull were carefully separated, a circular defect with a diameter of approximately 4–5 mm was drilled on both sides of the skull when the dura mater and brain tissue were protected.

Preparation of hyaluronic acid (HA) gel-encapsulated exosome

The preparation of HA gel-encapsulated exosomes in this study was slightly altered in the light of the previous study [27]. Briefly, after the hyaluronic acid powder was dissolved into deionized water to prepare 1% HA solution and the pH value of HA solution was adjusted by hydrochloric acid solution, the di-hydrazide adipate and carbodiimide hydrochloride were added one by one. Finally, after the sodium bicarbonate solution was employed to adjust the pH value to neutrality, the exosomes were added into the HA solution to prepare HA gel with different concentrations (5 μg/mL and 20 μg/mL) of the exosome.

Animal experiment protocol

According to the simple randomization procedure, all experimental rats were stochastically divided into the following five groups (n = 6): the blank, HA, HA + ADSCs, HA + Exo-H (20 μg/mL), and HA + Exo-L (5 μg/mL) groups. Rats in all divided groups suffered from the same surgical procedure, namely circular defects were established on their skull. After triumphantly establishing the cranial deficiency model, rats in the blank group were implanted with nothing, but rats in other groups were implanted with different materials into the cranial defects. Briefly, rats in the model + HA group were merely treated with hyaluronic acid (HA) gel, rats in the HA + ADSCs were treated with the mixture of HA gel and ADSCs, and rats in the HA + Exo-L and HA + Exo-H group were respectively treated with the mixture of HA gel and low-dose exosomes (5 μg/mL) or high-dose exosomes (20 μg/mL). After finishing the treatment for six weeks, all rats were anesthetized by sodium pentobarbital (40 mg/kg, i.p.) and sacrificed by the cervical dislocation approach, and the skull tissue from the defect sites was collected for subsequent studies. The work has been reported in line with the ARRIVE guidelines 2.0.

Micro-CT analysis

The samples of rats' skulls were scanned by adopting a micro-CT system (Bruker, Germany) and imaged by Data Viewer software (version 2.0). With the help of CtAn software (version 10.0), the areas of regions of interest were

extracted to contribute to further quantitative analysis of bone mineral density (BMD), percent bone volume (BV/TV), trabecular thickness (Tb.Th), and trabecular number (Tb.N) of skull samples. After that, the skull tissues were harvested from rats that were anesthetized with pentobarbital sodium and with euthanasia and adopted for subsequent studies.

Hematoxylin and eosin (H&E) staining

After the skull tissues were immersed in the 4% polyformaldehyde, they were decalcified by employing a 10% EDTA solution. Then, the decalcified skull tissues were embedded in paraffin to facilitate being cut into slices. All 4-μm thick slices were stained in hematoxylin for 5 min before they were transferred into 0.5% eosin for a further 3 min. After finishing staining, all sections were visualized to investigate the effects of ADSC-derived exosomes on the pathological injury of defect sites.

Masson staining

All 2-μm thick slices of skull tissue were dewaxed and chromized, they were successively transferred into hematoxylin for 10 min, ponceau for 10 min, 1% phosphomolybdic acid solution for 5 min, aniline blue for 5 min, and 1% glacial acetic acid for 1 min. Finally, all sections were observed to investigate the effects of ADSC-derived exosomes on the fibrosis of defect sites.

Immunohistochemical (IHC) staining

After the 2-μm thick slices were successfully dewaxed, they were first soaked in a citrate buffer solution to repair antigens. Then, 5% bovine serum albumin was adopted to prevent the non-specific binding for 30 min. All sections were incubated with the primary antibodies overnight at 4 ℃, including anti-ALP, anti-CD31, anti-Col-I, anti-OCN, anti-RUNX2, and anti-VEGFA, and then incubated with corresponding second antibodies for 30 min at room temperature. All slices were visualized to determine the effects of ADSC-derived exosomes on the expression level of these proteins in skull tissue.

Cell transfection

The lentivirus transfectants of mimics control, miR-21-5p mimics, inhibitors control, and miR-21-5p inhibitors were adopted for transfection on ADSCs. By employing the Lipofectamine 2000 reagent, the above three lentivirus transfectants were successfully transfected after being co-cultured with ADSCs for 48 h.

Cell experiment protocol

In the present study, the cell experiments were divided into two parts. One part was to investigate the effects of ADSC-derived exosomes on EPCs, and the other part was to explore the effects of exosomes extracted from ADSCs with transfection on EPCs. According to the simple randomization procedure, the former was divided into four groups, including the control, ADSCs, Exo-H (20 μg/mL), and Exo-L (5 μg/mL) groups, and the latter was divided into five groups, embracing the control, mimics control, miR-21-5p mimics, inhibitors control, and miR-21-5p inhibitors groups. For the former part, in the control group, there were only EPCs, but in the other three groups, the ADSCs, low-dose exosomes (5 μg/mL), and high-dose exosomes (20 μg/mL) were respectively co-cultured with EPCs for 48 h. For the latter part, apart from the control group, EPCs were co-cultured with exosomes transfected by corresponding lentivirus transfectants for 48 h in the mimics control, miR-21-5p mimics, inhibitors control, and miR-21-5p inhibitors groups.

Cell viability assay

After the EPCs in each group were seeded into a 96-well plate with a concentration of 3×10^4 cells/mL and suffered from the corresponding treatments, EPCs were incubated with 15 μL CCK-8 solution at 37 ℃ for a further 2 h. Finally, the optical density values under 450 nm of each group were recorded to determine the cell viability of EPCs.

Wound healing assay

After the EPCs were seeded into a 6-well plate with a concentration of 3×10^6 cells/mL for one night, a scratch with the same breadth was performed on each group. Then, the EPCs in each group suffered from the corresponding treatments for 48 h. The images of the same scratch site of each group were collected under a microscope before and after treatments, and the migration distances of EPCs in each group were quantified and analyzed with the help of the Image J software (version 1.8.0.112).

Transwell assay

The EPCs were seeded into the upper chamber of the 24-well Transwell plates with a concentration of 3×10^5 cells/mL. The culture medium, ADSCs, low-dose exosomes (5 μg/mL), and high-dose exosomes (20 μg/mL) were respectively added into the lower chamber of the 24-well Transwell plates. After the co-cultivation for 48 h, the EPCs in the upper chamber were fixed with 4% paraformaldehyde for 30 min and stained with crystal violet for 10 min. Finally, the stained EPCs were visualized by employing an optical microscope and analyzed by the Image J software.

Tube formation assay

The Matrigel was firstly diluted with culture medium in a proportion of 1: 3, and then the diluted Matrigel was added to coat the plates. After the corresponding treatments for 48 h were offered to EPCs, EPCs in each group were seeded on the plates coated with Matrigel for 8 h. Finally, the optical microscope was adopted to observe and determine the tube formation of EPCs.

Dual-luciferase report

The binding sites between miR-21-5p and NOTCH1 were first predicted with the help of miRDB (http://mirdb.org/). The pmirGLO carriers loaded by the wild-type and mutant-type sequence of NOTCH1 3′UTR (NOTCH1 3′UTR wt and NOTCH1 3′UTR mut) were provided by Sangon Biotech (Shanghai, China). After the NC mimics and miR-21-5p mimics were respectively transfected into EPCs, the luciferase activity was measured.

RT-PCR

After the Trizol reagent was applied to extract the total RNAs in EPCs, ADSCs, and ADSC-derived exosomes triumphantly, with the help of the PCR system, the reverse transcription kit and the QPCR reaction kit were used to transcribe total RNAs into cDNAs reversely and achieve the amplification of DNA. According to the cycle threshold, the approach of $2^{-\Delta\Delta Ct}$ was adopted to calculate the mRNA expression level of each gene. The employed primer sequences are listed in Table 1.

Western blot

After the total proteins in EPCs and ADSC-derived exosomes were extracted by RIPA lysis buffer. Then, the protein samples denatured by boiling water were loaded on the sodium dodecyl sulfate–polyacrylamide gel for separation with the help of electrophoresis. After that, the separated protein samples were transferred to the polyvinylidene fluoride membranes. After the membranes were blocked by 5% bovine serum albumin for 1 h, they were further incubated with primary antibodies, including anti-CD9, anti-CD63, anti-CD31, anti-VEGFA, anti-OCN, anti-RUNX2, anti-NOTCH1, and anti-DLL4 at 4 ℃ for one night, then were immersed in the second antibodies for further 1 h at 37 ℃. Before imaging with the chemiluminescence instrument, the membranes were stained by the enhanced chemiluminescence. The Image J software was applied to analyze the grayscale value of blots to determine the expression level of proteins.

Statistical analysis

All experiments in vivo and in vitro were repeated three times. All generated data in vivo and in vitro were included in the statistical analysis. The experimental data were analyzed by employing the GraphPad (v: 8.0.2) software, expressed in the form of mean ± standard deviation, and presented in the form of a figure. After the Shapro-Wilk testing was employed to determine the normal distribution of data, the least significant difference test was used for pairwise comparisons between multiple groups. $P < 0.05$ means significant statistical differences.

Results

Identification and internalization of exosomes

After the particles were triumphantly extracted from ADSCs, approaches of TEM, NTA, and Western blot were adopted for the characterization of exosomes together. As Fig. 1A shows, the extracted particles present spherical structures with a concave center and a complete cell membrane structure under the vision of TEM. Meanwhile, the analysis results of the particle size distribution detected by NTA suggested the average diameter of extracted particles is 126 nm, which is in accord with the diameter range of exosomes (Fig. 1B). In addition, as Fig. 1C presents, the expression levels of exosomal markers, namely CD9 and CD63, in the extracted particles

Table 1 The primer sequence of all genes for RT-PCR

Gene	Forward	Reverse
CD31	CACCGTGATACTGAACAGCAA	GTCACAATCCCACCTTCTGTC
VEGFA	CCCTGGCTTTACTGCTGTAC	TCTGAACAAGGCTCACAGTG
OCN	CCTCACACTCCTCGCCCTATT	CCCTCCTGCTTGGACACAAA
RUNX2	ACTTCCTGTGCTCGGTGCT	GACGGTTATGGTCAAGGTGA
miR-21-5p	TCGCTCGAGATTTTTTTTTATCAAGAGGG	TCGGCGGCCGCGACAAGAATG AGACTTTAATC
NOTCH1	TCGGAGTGGACAGGTCAGTA	AGATACACGCATCGTTCAGG
DLL4	TGCGGATAACCAACGACG	GCCCACAAAGCCATAAGGAC
U6	TCGGCGGCCGCGACAAGAATGAGACTTTAATC	CGCTTCACGAATTTGCGTGTCAT
β-actin	GAGAGGGAAATCGTGCGTGA	GCCTAGAAGCATTTGCGGTG

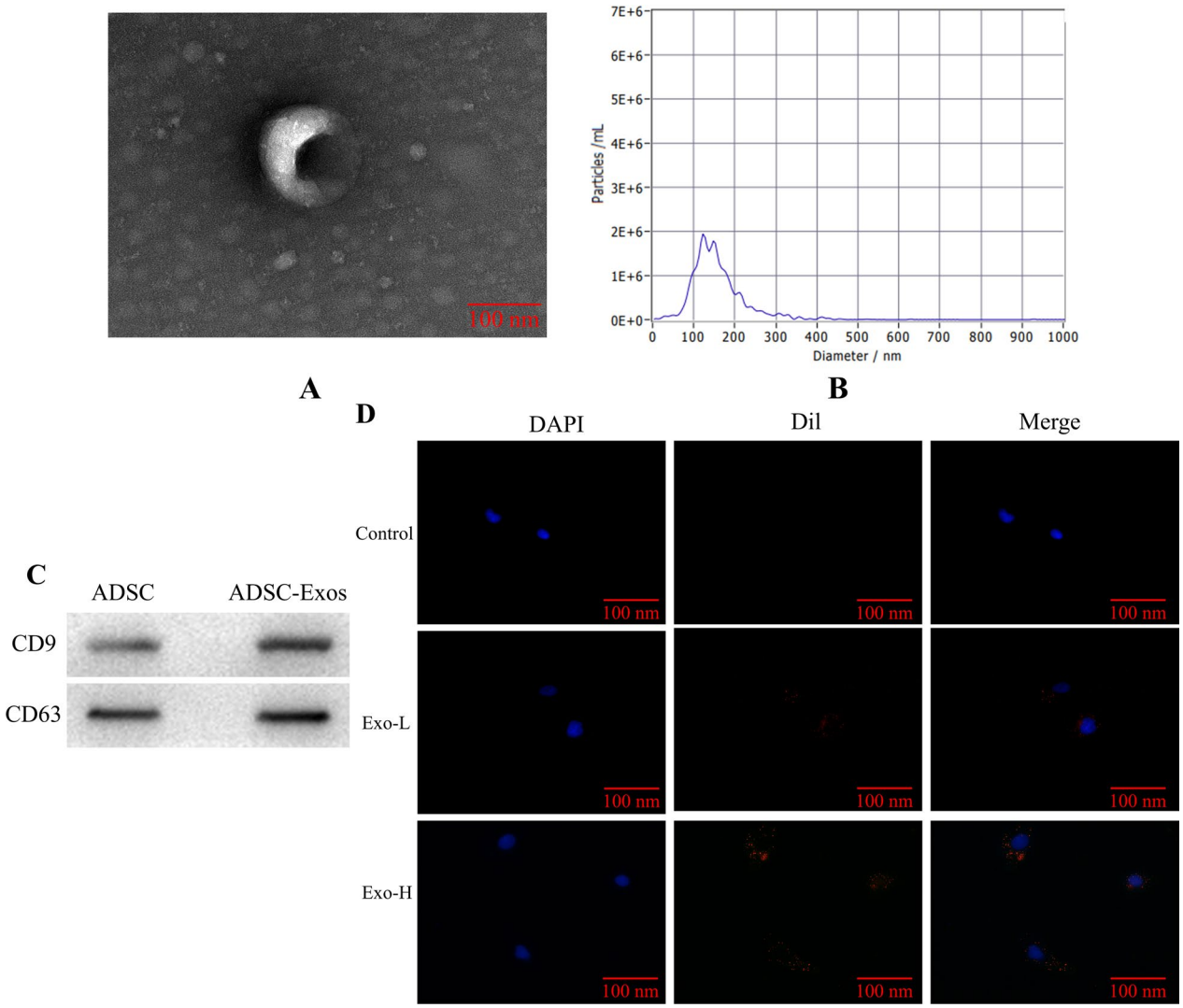

Fig. 1 The results of the identification and internalization of exosomes. The morphology of extracted particles under TEM (**A**). The particle size distribution of extracted particles detected by NTA (**B**). The expression level of exosomal markers, CD9 and CD63, in extracted particles and ADSCs (**C**). Representative fluorescent images of the internalization of ADSC-derived exosomes in EPCs (**D**)

were higher than those in ADSCs. As shown in Fig. 1D, all EPC cells were stained in blue by the DAPI solution, and ADSC-derived exosomes were stained in red by the Dil solution. The ADSC-derived exosomes were accumulated around EPC cells, suggesting the exosomes were gradually internalized by EPC cells. All in all, the above results indicated that the particles extracted from ADSCs in this study belonged to exosomes and could be internalized by EPC cells.

Effects of ADSC-derived exosomes on repairment of cranial defects and micro-CT analysis results

After finishing the corresponding treatments for 6 weeks, the status of cranial defects in each group was recorded, detected, and evaluated before collecting skull tissues with the help of a camera and micro-CT analysis. As Fig. 2A, B illustrate, there is almost no new bone formation in the cranial defects of the blank group, there is slight new bone formation in the cranial defects of the HA and HA + ADSCs groups, and there is massive new bone formation in the cranial defects of the HA + Exo-L and HA + Exo-H groups. Moreover, based on the micro-CT analysis, the bone-related parameters in each group, including BMD, BV/TV, Tb.Th, and Tb.N, present the same altered tendency. As Fig. 2C–F shows, there is no significant difference of the above four parameters between the blank group and the HA group. Compared with the blank group, the levels of the above four

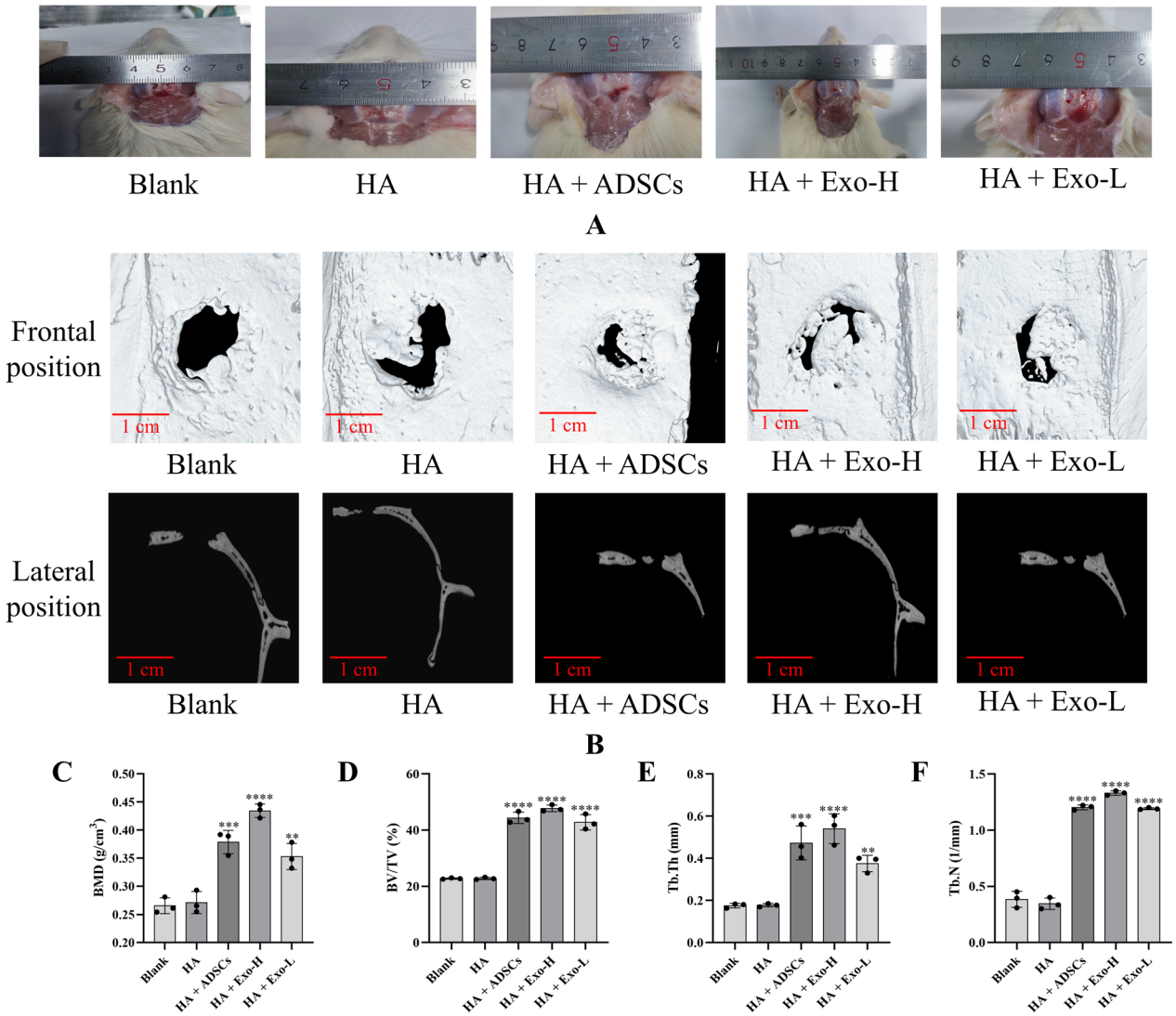

Fig. 2 Effects of ADSC-derived exosomes on repairment of cranial defects and micro-CT analysis results. The images of cranial defects in each group before collecting skull tissues (**A**). The 3D reconstruction images of cranial defects in each group from the frontal and lateral positions (**B**). The statistical analysis of bone-related parameters based on the micro-CT analysis, embracing BMD (**C**), BV/TV (**D**), Tb.Th (**E**), and Tb.N (**F**) (n = 3). All generated data were included in the statistical analysis. ****/***/** $p < 0.0001/0.001/0.01$ vs. Blank

parameters were all dramatically up-regulated in the HA + ADSCs, HA + Exo-L, and HA + Exo-H groups. It indicated that ADSC-derived exosomes accelerate the repairment of cranial defects.

Effects of ADSC-derived exosomes on the histopathology and fibrosis of cranial defect tissues

As the restorative effects of ADSC-derived exosomes on cranial defects have been preliminarily confirmed, the H&E staining and Masson staining were further adopted to further evaluate the effects of ADSC-derived exosomes on cranial defects from the level of histology. Illustrated in Fig. 3A, the nascent vascular and bone tissues in the blank group were the least compared with the other intervention groups. Meanwhile, the further administration of ADSCs and ADSC-derived exosomes contributed to repairing cranial defects, among which the high-dose of exosomes possessed the strongest therapeutic ability on cranial defects. Moreover, as Fig. 3B displays, the blue stained parts represent the newly formed bone tissues and the red stained parts represent the mature bone tissues. The results of Masson staining indicated that there was no significant difference in the area of blue stained parts between the blank and HA groups. The area of blue stained parts in the HA + ADSCs, HA + Exo-L, and HA + Exo-H groups were larger than those in the blank

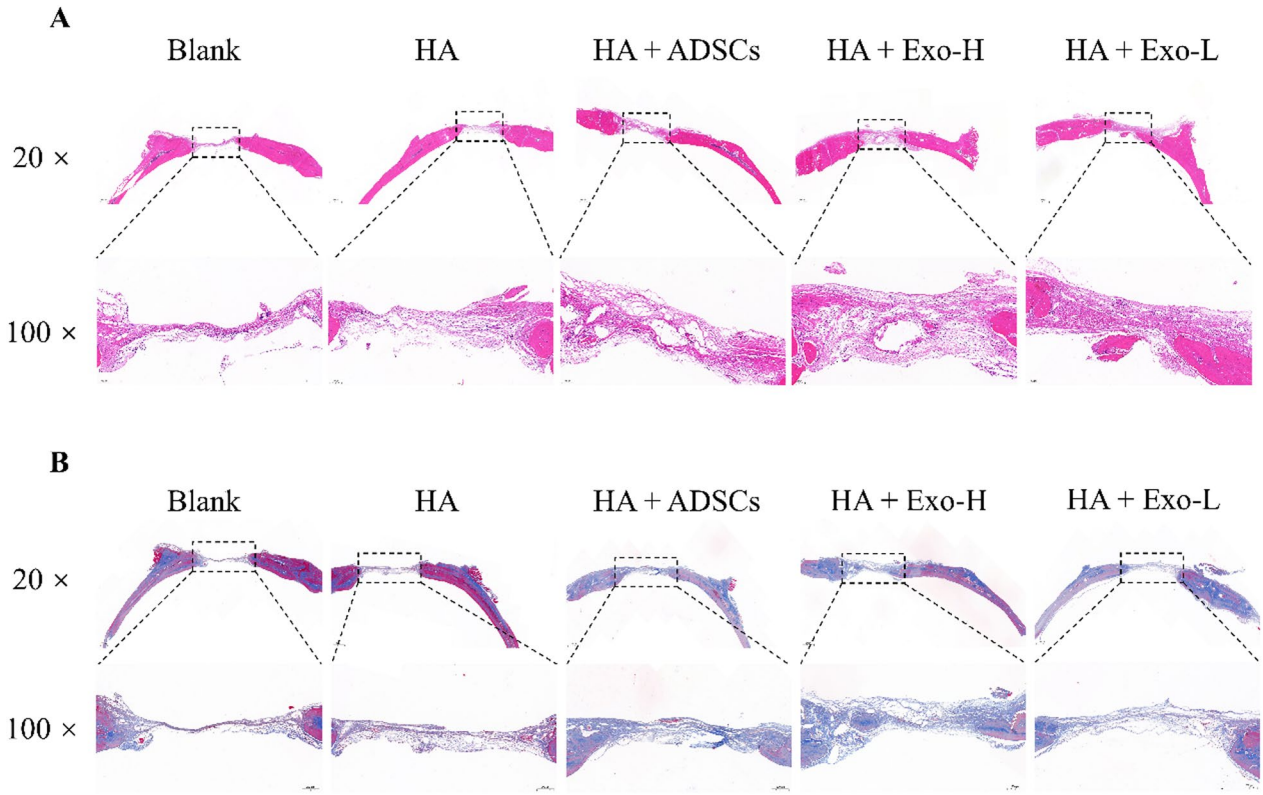

Fig. 3 Effects of ADSC-derived exosomes on the histopathology and fibrosis of cranial defect tissues. The representative images of H&E staining of cranial defect tissues with the magnification of 20 × and 100 × (**A**). The representative images of Masson staining of cranial defect tissues with the magnification of 20 × and 100 × (**B**)

or HA group. The above results collectively suggested that ADSC-derived exosomes facilitate the repair of cranial defects by accelerating the revitalization of vascular and bone tissues.

Effects of ADSC-derived exosomes on the expression of related genes and proteins in cranial defect tissues

Due to the above results of histological staining demonstrating the therapeutic effects of ADSC-derived exosomes on cranial defects, we next determine the expression of genes and proteins related to the revitalization of vascular and bone tissues to further investigate the effects of ADSC-derived exosomes at the molecular level. As Fig. 4A-E shows, the results of IHC indicated that the expression levels of related proteins (including CD31, VEGFA, OCN, and RUNX2) all elevated in the HA + ADSCs, HA + Exo-L, and HA + Exo-H groups compared with the blank group. In addition, the RT-PCR and Western blot technologies were adopted to determine the gene and protein expression levels of CD31, VEGFA, OCN, and RUNX2 in cranial defect tissues. As Fig. 5A–I present, compared with the blank group, the gene and protein expression levels of the above indicators were both significantly up-regulated, among which the gene and protein expression levels of all indicators in the HA + Exo-H group are the highest.

Effects of ADSC-derived exosomes on the cell viability, migration, invasion, and tube formation of EPCs

Owing to the therapeutic effects of ADSC-derived exosomes on cranial defects having been confirmed in vivo, we further determined the effects of ADSC-derived exosomes on EPCs in vitro. As Fig. 6A–G presents, the altered tendencies of cell viability, migration, invasion, and tube formation of EPCs were the same after being co-cultured with ADSCs or treated by ADSC-derived exosomes. The cell viability, relative migration rate, number of invaded cells, and number of tube formations in the ADSCs, Exo-L, and Exo-H groups were all significantly elevated compared with those in the control groups. The above results suggested that the co-cultivation with ADSCs and the incubation with ADSC-derived exosomes both improved the cell viability, migration ability, invasion ability, and tube formation ability of EPCs in vitro.

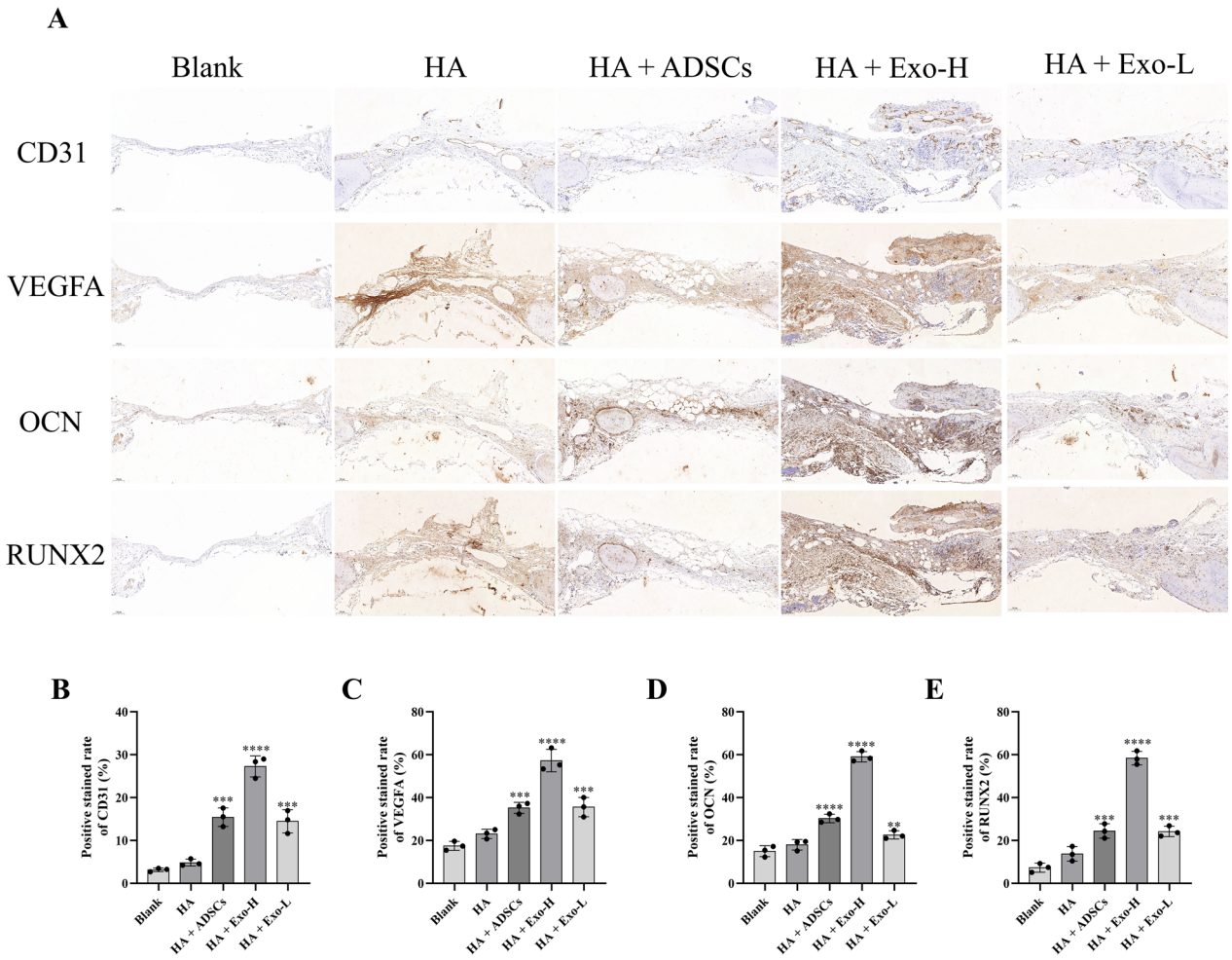

Fig. 4 Effects of ADSC-derived exosomes on the expression of related proteins in cranial defect tissues. The representative images of IHC of related proteins (i.e., CD31, VEGFA, OCN, and RUNX2) in cranial defect tissues (**A**). The statistical analysis of the positive stained rate of CD31 (**B**), VEGFA (**C**), OCN (**D**), and RUNX2 (**E**) in cranial defect tissues (n = 3). All generated data were included in the statistical analysis. ****/***/** $p < 0.0001/0.001/0.01$ vs. Blank

Effects of ADSC-derived exosomes on the expression of related genes and proteins in EPCs

Since the improvement effects of ADSC-derived exosomes on the cell viability, migration ability, invasion ability, and tube formation ability of EPCs has been verified, we further investigate the effects of ADSC-derived exosomes on EPCs in vitro at the molecular level by employing RT-PCR and Western blot technologies. As Fig. 7A–E show, the gene and protein expression levels of angiogenesis-related genes in EPCs, embracing CD31 and VEGFA, both were prominently up-regulated when co-culturing with ADSCs or ADSC-derived exosomes compared with those in the control group. The above results further suggest angiogenesis is involved in the effects of ADSC-derived exosomes on EPCs.

Identification of the miRNA with the highest expression level in ADSC-derived exosomes and its downstream target

So far, the effects of ADSC-derived exosomes on cranial defect tissues in vivo and EPCs in vitro have already been demonstrated, but which miRNAs are involved in these regulations is thought-provoking. The miRNAs with high expression in ADSC-derived exosomes were first determined with the help of gene sequencing. As Fig. 8A presents, 20 kinds of miRNAs are highly expressed in ADSC-derived exosomes, among which the expression level of miR-21-5p is the highest. As Fig. 8B shows, the results of the Venn diagram showed that there were 17 same miRNAs among the miRanda, RNAhybird, Targetscan, and our gene sequencing results, in which include miR-21-5p. The expression levels of miRNAs in the top five in ADSCs and ADSC-derived exosomes as

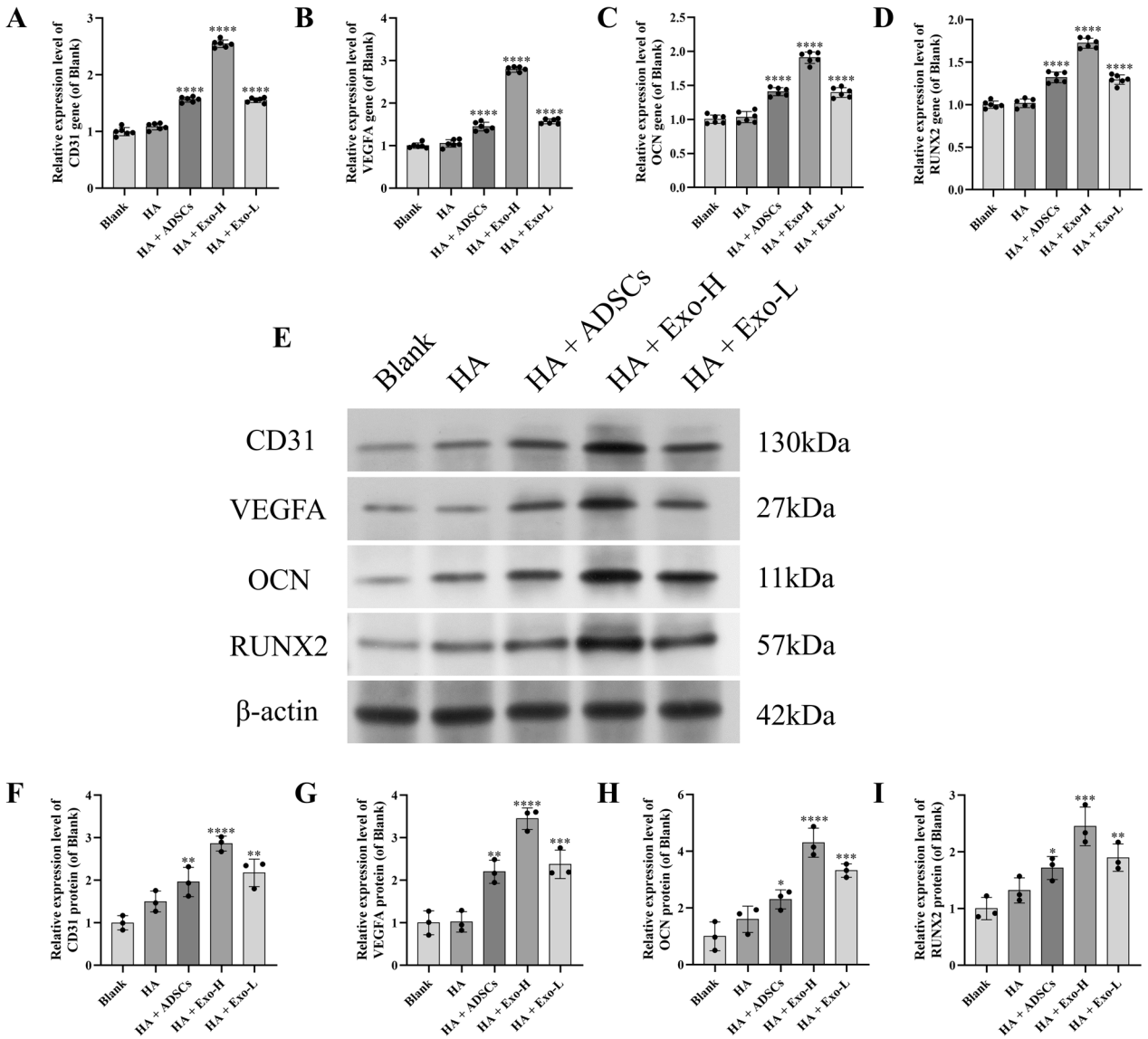

Fig. 5 Effects of ADSC-derived exosomes on the expression of related genes and proteins in cranial defect tissues. The statistical analysis of the gene expression level of CD31 (**A**), VEGFA (**B**), OCN (**C**), and RUNX2 (**D**) in cranial defect tissues (n = 6). The representative images of protein blots of CD31, VEGFA, OCN, RUNX2, and β-actin in cranial defect tissues (**E**). The statistical analysis of the protein expression level of CD31 (**F**), VEGFA (**G**), OCN (**H**), and RUNX2 (**I**) in cranial defect tissues (n = 3). All generated data were included in the statistical analysis. $^{****/***/**}p < 0.0001/0.001/0.01$ vs. Blank

well as the expression level of miR-21-5p in EPCs after co-culturing with ADSCs or ADSC-derived exosomes were respectively determined by employing RT-PCR technology. As Fig. 8C shows, the expression of the top five miRNAs, namely miR-21-5p, let-7i-5p, let-7b-5p, let-7c-5p, and miR-26a-5p were all detected in ADSCs and ADSC-derived exosomes, among which the expression level of miR-21-5p in ADSC-derived exosomes was the highest. Meanwhile, as Fig. 8D illustrates, after the co-cultivation with ADSCs or ADSC-derived exosomes, the expression level of miR-21-5p in EPCs was dramatically up-regulated, and the expression level of miR-21-5p in EPCs after co-culturing with ADSC-derived exosomes was higher. The above results indicated that miR-21-5p was the miRNA with the highest expression level in ADSC-derived exosomes. With the help of the dual-luciferase report experiment, the downstream target of miR-21-5p was identified. As shown in Fig. 8E, there were potential binding sites between 3'-UTR in NOTCH1 and miR-21-5p. In addition, as Fig. 8F shows, although

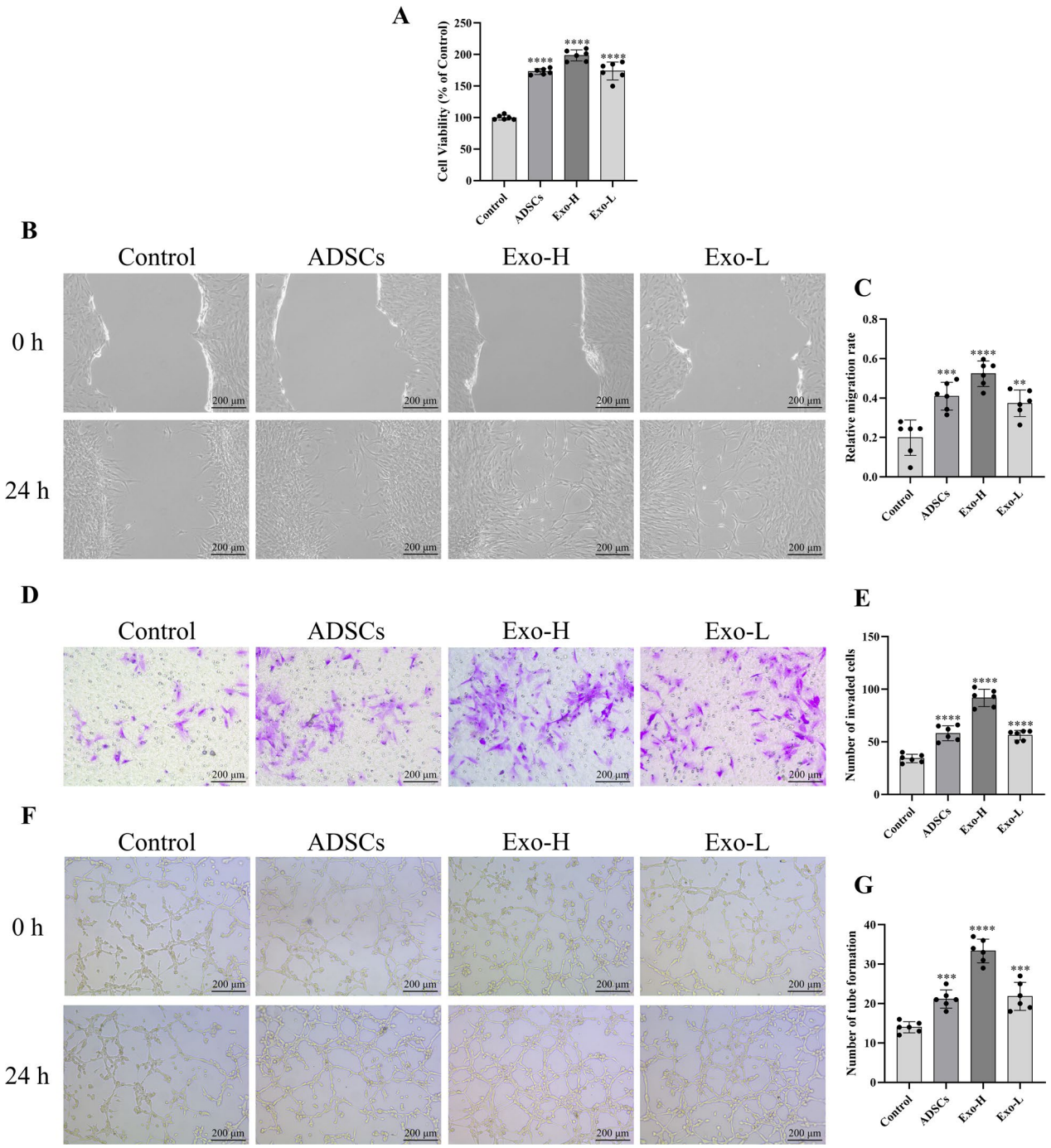

Fig. 6 Effects of ADSC-derived exosomes on the cell viability, migration, invasion, and tube formation of EPCs. The statistical analysis of cell viability of EPCs (**A**) (n = 6). The representative images of wound healing assay of EPCs (**B**). The statistical analysis of the relative migration rate of EPCs (**C**) (n = 6). The representative images of transwell assay of EPCs (**D**). The statistical analysis of the number of invaded EPCs (**E**) (n = 6). The representative images of tube information assay of EPCs (**F**). The statistical analysis of number of tube formation of EPCs (**G**) (n = 6). All generated data were included in the statistical analysis. ****/***/** $p < 0.0001/0.001/0.01$ vs. Control

the miR-21-5p mimics could not influence the fluorescence intensity of NOTCH1 3'UTR mut, the miR-21-5p mimics significantly reduced the fluorescence intensity of NOTCH1 3'UTR wt. The above results indicated that NOTCH1 was the potential downstream target of miR-21-5p.

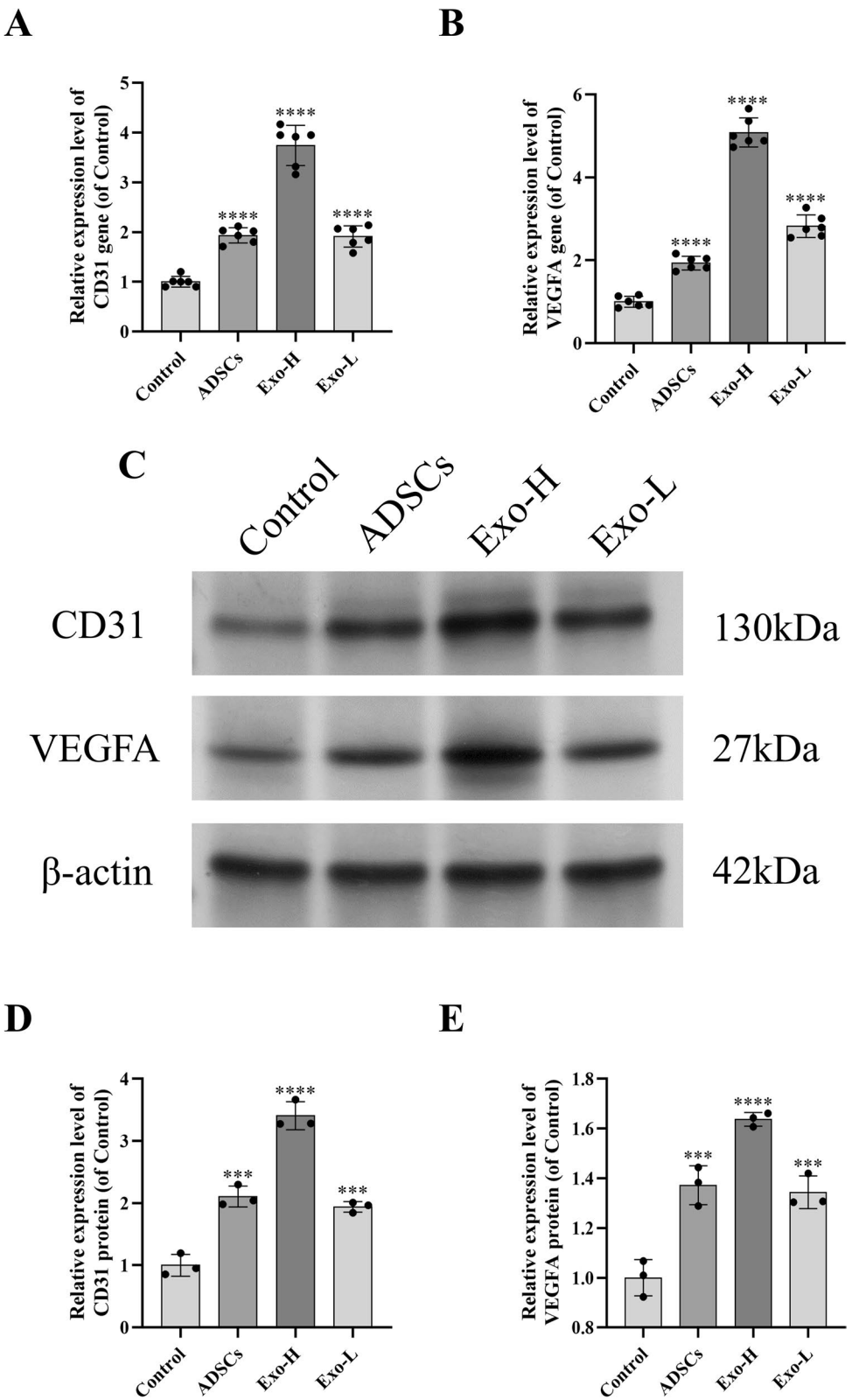

Fig. 7 Effects of ADSC-derived exosomes on the expression of related genes and proteins in EPCs. The statistical analysis of the gene expression level of CD31 (**A**) and VEGFA (**B**) in EPCs (n = 6). The representative images of protein blots of CD31, VEGFA, and β-actin in EPCs (**C**). The statistical analysis of the protein expression level of CD31 (**D**) and VEGFA (**E**) in EPCs (n = 3). All generated data were included in the statistical analysis. ****/*** $p < 0.0001/0.001$ vs. Control

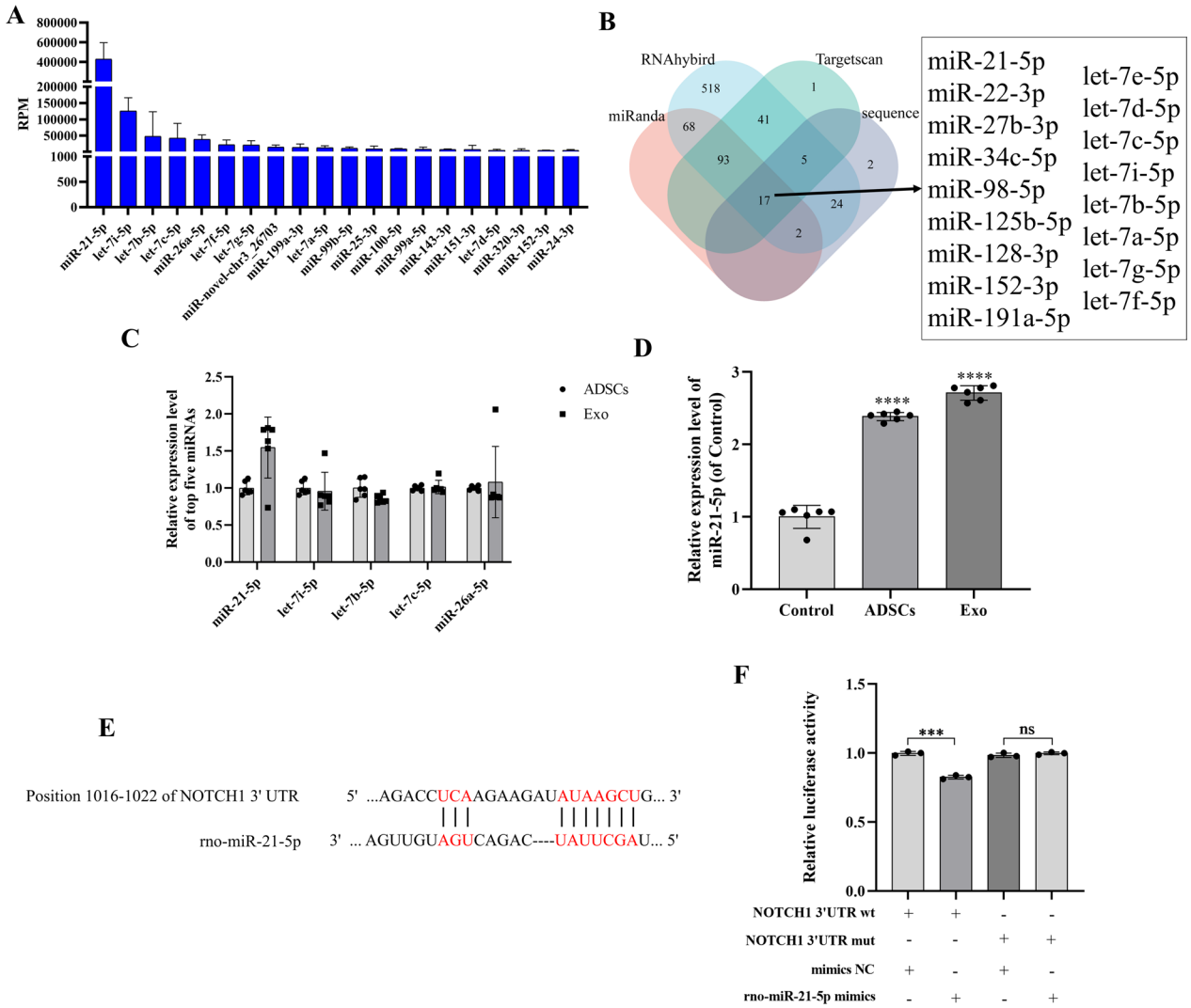

Fig. 8 Identification of the miRNA with the highest expression level in ADSC-derived exosomes and its downstream target. The results of the top twenty miRNAs with high expression in the ADSC-derived exosomes were detected by gene sequencing (**A**). The Venn diagram among the miRanda, RNAhybird, Targetscan, and our gene sequencing results (**B**). The statistical analysis of the expression level of the top five miRNAs (i.e., miR-21-5p, let-7i-5p, let-7b-5p, let-7c-5p, and miR-26a-5p) with high expression in ADSCs and ADSC-derived exosomes (**C**) (n = 6). The statistical analysis of the gene expression level of miR-21-5p in EPCs (**D**) (n = 6). The predicted results of the binding site between miR-21-5p and NOTCH1 (**E**). The results of the dual-luciferase report experiment between miR-21-5p and NOTCH1 (**F**) (n = 3). All generated data were included in the statistical analysis. $^{****}p < 0.0001$ vs. Control, $^{***}p < 0.001$ vs. the first group

Effects of miR-21-5p in ADSC-derived exosomes on the migration and tube formation of EPCs

The RT-PCR technology was first adopted to determine whether the control oligonucleotide, miR-21-5p mimics, and miR-21-5p inhibitors were successfully transfected into ADSC-derived exosomes. As Fig. 9A displays, compared with the mimics control or inhibitors control group, the relative expression level of miR-21-5p in ADSC-derived exosomes was prominently up-regulated in the miR-21-5p mimics group but was memorably down-regulated in the miR-21-5p inhibitors group. The above results suggested that all transfectants were successfully transfected into ADSC-derived exosomes. After that, we investigate the effects of miR-21-5p in ADSC-derived exosomes on the migration and tube formation of EPCs. The altered tendencies of migration and tube formation of EPCs after co-culturing with exosomes incubated with different transfectants were the same as those of the expression level of miR-21-5p above. As Fig. 9B–E present, the relative migration rate and the number of tube formations

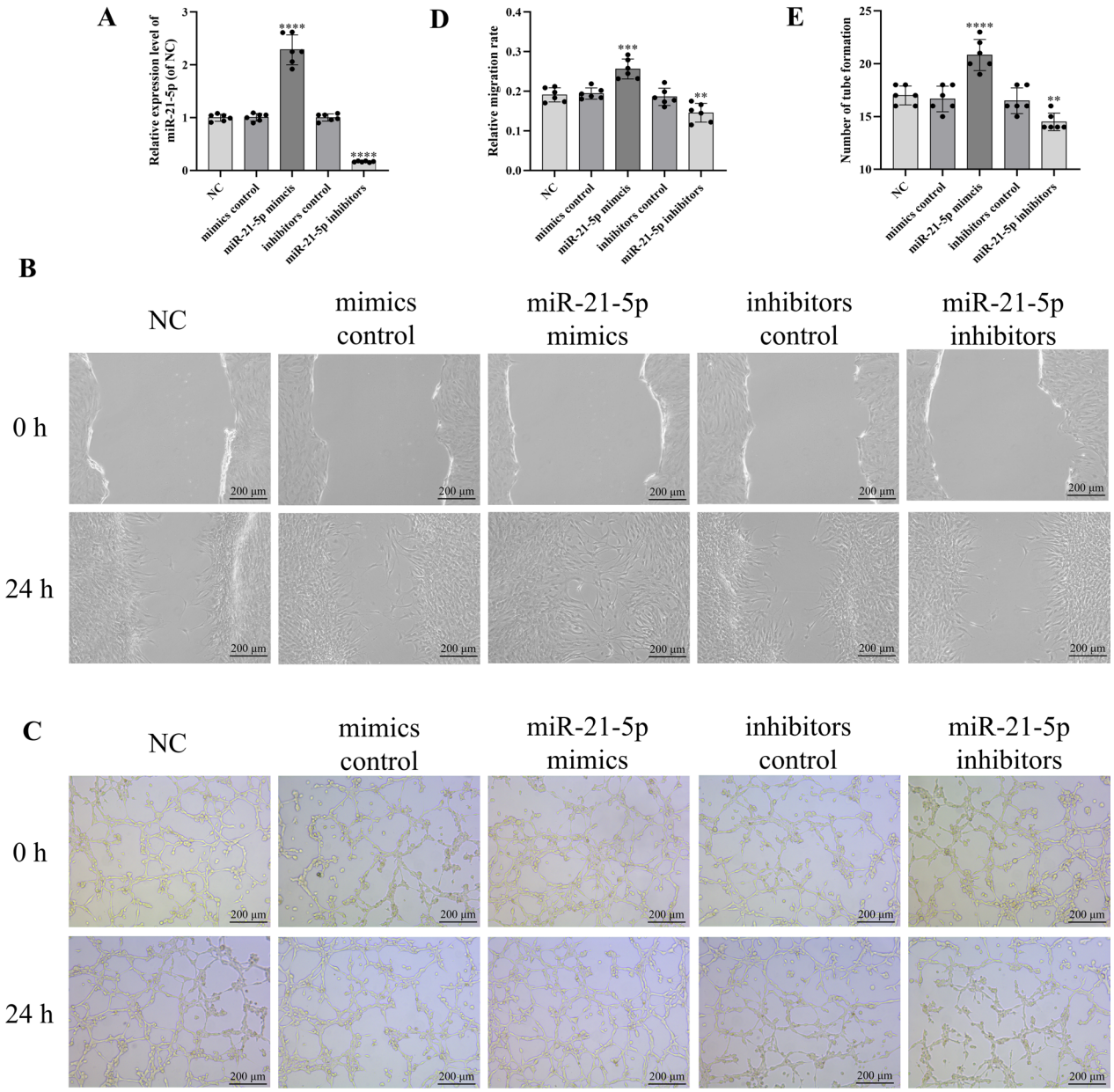

Fig. 9 Effects of miR-21-5p in ADSC-derived exosomes on the migration and tube formation of EPCs. The statistical analysis of the expression level of miR-21-5p in EPCs after transfection (**A**) (n = 6). The representative images of wound healing assay of EPCs after transfection (**B**). The statistical analysis of the relative migration rate of EPCs after transfection (**C**) (n = 6). The representative images of tube information assay of EPCs after transfection (**D**). The statistical analysis of the number of tube formation of EPCs after transfection (**E**) (n = 6). All generated data were included in the statistical analysis. $^{****/**}p < 0.0001/0.01$ vs. NC

were significantly elevated because of transfecting miR-21-5p mimics ADSC-derived exosomes but were substantially declined since the transfection of miR-21-5p inhibitors. The above results imply that miR-21-5p in ADSC-derived exosomes plays an essential role in promoting the ability of migration and tube formation of EPCs.

Effects of miR-21-5p in ADSC-derived exosomes on the NOTCH1/DLL4/VEGFA signaling pathway of EPCs

The effects of miR-21-5p in ADSC-derived exosomes on the NOTCH1/DLL4/VEGFA signaling pathway of EPCs were further investigated because it has been affirmed that NOTCH1 was the potential downstream target of miR-21-5p. The gene and protein expression levels of VEGFA, NOTCH1, and DLL4 of EPCs after co-culturing with exosomes transfected with miR-21-5p mimics or miR-21-5p inhibitors were determined by RT-PCR and Western-blot technologies, respectively. As Fig. 10A, E present, the gene and protein expression levels of VEGFA of EPCs were dramatically up-regulated after transfecting with miR-21-5p mimics and were significantly down-regulated after transfecting with miR-21-5p inhibitors. Moreover, as shown in Fig. 10B, C, F, G, the gene and protein expression levels of NOTCH1 and DLL4 were prominently down-regulated after transfecting with miR-21-5p mimics and were substantially up-regulated after transfecting with miR-21-5p inhibitors. The above results demonstrated that miR-21-5p in ADSC-derived exosomes promoted bone repair by regulating the NOTCH1/DLL4/VEGFA signaling pathway.

Discussion

In recent years, bone tissue engineering based on scaffolds, factors, and stem cells has gradually become a hot topic in repairing and treating bone defects [28]. Exosomes in stem cells, a kind of small membrane bubbles containing cell-specific proteins, lipids, and nucleic acids, have been demonstrated to regulate the microenvironment of angiogenesis to accelerate bone repair [29, 30]. One previous study indicated that human serum-derived exosomes up-regulated the expression of CD31 to promote angiogenesis, contributing to bone regeneration [31]. It was also reported that mesenchymal stem cell-derived exosomes enhanced osteogenesis reflected by up-regulating the expression of osteogenesis-related markers OCN and RUNX2 [32]. Although many studies have proved the promoted effects of exosomes derived from different cells on angiogenesis and osteogenesis, studies on the effects and mechanisms of ADSC-derived exosomes on angiogenesis to promote bone repair are still few. In addition, it was demonstrated that EPC induces angiogenesis and vascular repair to enhance bone fracture healing by differentiating into mature endothelial cells [33]. Therefore, this study investigated the effects of ADSC-derived exosomes on angiogenesis in vivo and on EPCs in vitro. The present study's findings confirmed that ADSC-derived exosomes promoted angiogenesis to accelerate bone repair by enhancing the activity of EPCs. In vivo, ADSC-derived exosomes enhanced the revitalization of bone tissue, up-regulated the gene and protein expression levels of CD31, VEGFA, OCN, and RUNX2, and promoted the repairment of cranial defects, indicating promoted new bone formation by promoting angiogenesis at cranial deficiency sites to enhance osteoblast activity. In vitro, ADSC-derived exosomes promoted cell viability, migration, invasion, tube formation, and expression of growth factors (including CD31 and VEGFA) that promote angiogenesis in EPCs, suggesting ADSC-derived exosomes facilitated the potentiality of angiogenesis of EPCs. Moreover, the previous study has affirmed that ADSC-derived exosomes regulate angiogenesis by the miR-146a-5p/JAZF1 axis in human umbilical vein endothelial cells (HUVECs) [34]. Compared with this study, our study innovatively demonstrated the effects and mechanisms of ADSC-derived exosomes on EPCs.

The effects of ADSC-derived exosomes on HUVECs may be original from their effects on EPCs because EPC induces angiogenesis and vascular repair by differentiating into mature endothelial cells [33]. In addition, the number of administrated ADSCs is a critical factor in this study. The bone repair effects will be weakened if insufficient ADSCs are treated, leading to the comparison in the effects on bone repair between ADSCs and exosomes becoming invalid. Meanwhile, the excessive ADSCs may induce adipose tissue formation around the bone repair region, resulting in the delay of bone repair progression. In this study, we observed a potentially interesting phenotype, namely the adipose tissue formed in the bone repair region of the HA + ADSCs group (seen in Fig. 4A). The formed adipose tissue may affect the local blood supply and secrete various cytokines to mediate inflammatory response during bone healing, retarding the bone repair progression [35, 36]. Therefore, we consider those are the reasons why exosome-based treatments are superior to ADSC transplantation in bone repair. Certainly, we believe that the mechanisms by which exosome-based treatments are superior to ADSC transplantation deserve further exploration.

Although the effects of ADSC-derived exosomes on angiogenesis in vivo and in vitro were confirmed in this study, their mechanisms were still unclear. Therefore, in the subsequent studies, the mechanisms of ADSC-derived exosomes in promoting angiogenesis were further investigated. It was reported that miRNAs contained in exosomes participate in regulating the biological activity of target cells by specifically binding to the messenger RNA to regulate the translation of proteins [37]. Some previous studies demonstrated that different miRNAs, such as miR-21-3p, miR-126-3p, and miR-519-3p, derived from various kinds of cells all improved angiogenesis [38–41]. Moreover, previous studies affirmed that miR-181b-5p and miR-126-3p in ADSC-derived

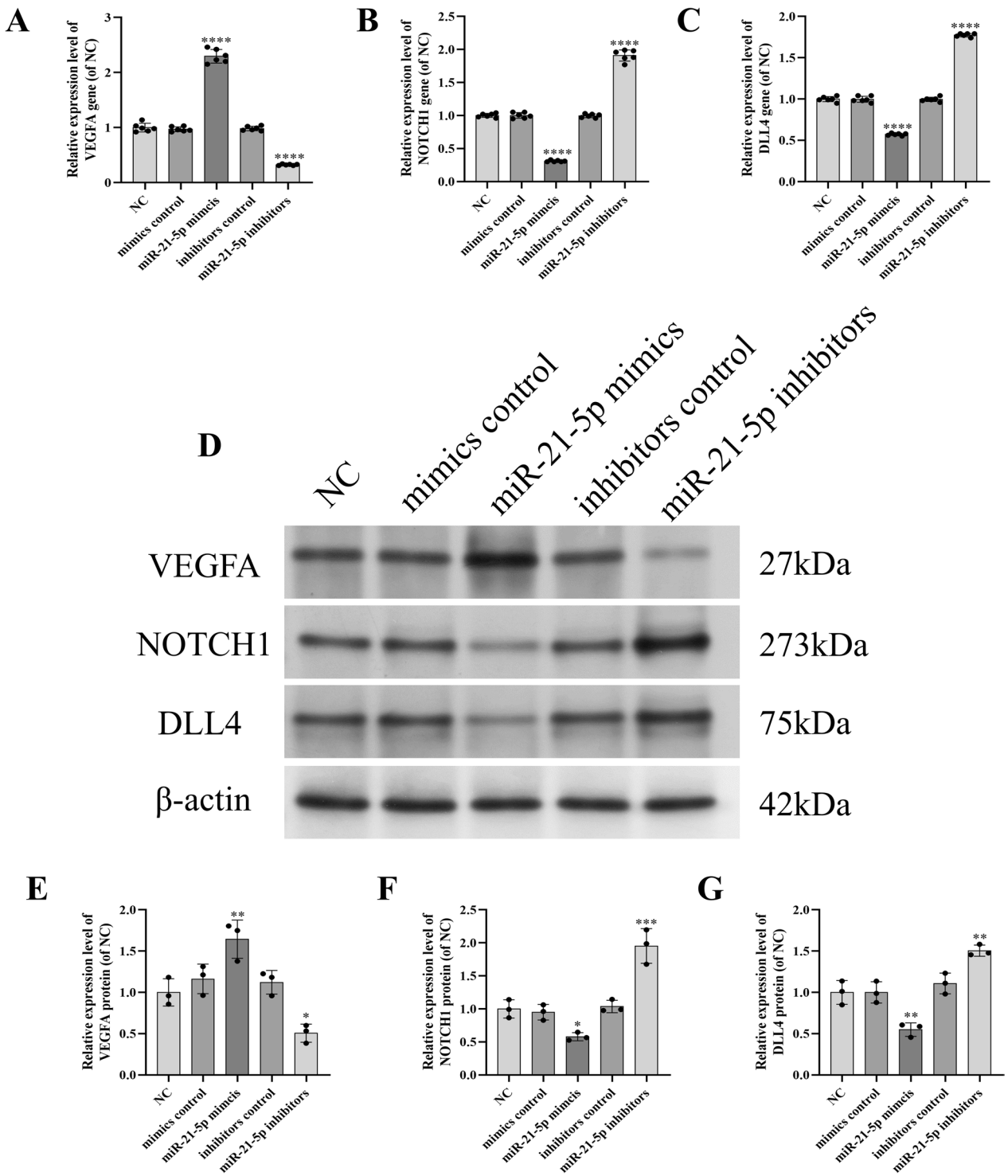

Fig. 10 Effects of miR-21-5p in ADSC-derived exosomes on the NOTCH1/DLL4/VEGFA pathway in EPCs. The statistical analysis of the gene expression level of VEGFA (**A**), NOTCH1 (**B**), and DLL4 (**C**) in EPCs (n = 6). The representative images of protein blots of HIF-1α, VEGFA, NOTCH1, DLL4, and β-actin in EPCs (**D**). The statistical analysis of the protein expression level of VEGFA (**E**), NOTCH1 (**F**), and DLL4 (**G**) in EPCs (n = 3). All generated data were included in the statistical analysis. ****/***/**/* $p < 0.0001/0.001/0.01/0.05$ vs. NC

exosomes were respectively conducive to the angiogenesis of brain microvascular endothelial cells and human umbilical vein endothelial cells, which were reflected as up-regulating the expression of HIF-1α and VEGFA [42, 43]. However, there were few studies investigated the effects of miR-21-5p in ADSC-derived exosomes on angiogenesis. Therefore, in the present study, we innovatively investigated the effects of miR-21-5p in ADSC-derived exosomes on angiogenesis. The gene sequencing of exosomes, bioinformatics analysis, and RT-PCR collectively affirmed that miR-21-5p was the highest expressed in ADSC-derived exosomes. The expression level of miR-21-5p in EPCs was also dramatically up-regulated after co-culturing with ADSC-derived exosomes. In addition, the migration and tube formation of EPCs were up-regulated and down-regulated after co-culturing with ADSC-derived exosomes transfected with miR-21-5p mimics or miR-21-5p inhibitors. Although the discovered miRNA in ADSC-derived exosomes that could enhance angiogenesis in this study was different from the previous studies, the above results also demonstrated that miR-21-5p of ADSC-derived exosomes played an essential role in promoting angiogenesis.

The NOTCH signaling pathway participates in multiple steps of angiogenesis, playing a crucial role in the occurrence and development of ischemic cardiovascular and cerebrovascular diseases, tumors, and bone defects [44–47]. Moreover, the overexpression of VEGFA regulated by the NOTCH signaling pathway increases endothelial cell proliferation, migration, and angiogenesis [48]. Meanwhile, the DLL4 protein, an important receptor of the NOTC1, also contributes to regulating biological processes, such as angiogenesis [49]. Besides, the effects of the NOTCH1/DLL4 signaling pathway on angiogenesis vary depending on different situations. It has been affirmed that the activation of the NOTCH1/DLL4 signaling pathway promoted angiogenesis during embryonic vascular development [50]. However, in the progression of cancers and bone repair, the activation of the NOTCH1/DLL4 signaling pathway inhibited their angiogenesis [27, 51]. In addition, the previous studies affirmed that exosome-derived miR-148b-3p inhibited the expression of NOTCH1 and DLL4 to promote angiogenesis, alleviating cerebral ischemia injuries [52]. It was demonstrated that exosome-derived miR-424-5p also negatively regulated the NOTCH1/DLL4 signaling pathway to facilitate angiogenesis, enhancing endometrial injury repair [53]. However, the effects of miR-21-5p in ADSC-derived exosomes on the NOTCH1/DLL4 signaling pathway are still unclear. Therefore, after the role of miR-21-5p of ADSC-derived exosomes in promoting angiogenesis was proved, the effects of miR-21-5p on the NOTCH1/DLL4/VEGFA signaling pathway in EPCs after co-culturing with ADSC-derived exosomes transfected with miR-21-5p mimics or miR-21-5p inhibitors were further investigated. The predicted results of miRDB and the experimental results of the dual-luciferase report collectively indicated that NOTCH1 was the downstream target of miR-21-5p. Meanwhile, the results of RT-PCR and Western blot also indicated that the overexpression of miR-21-5p up-regulated the gene and protein expression levels of VEGFA and down-regulated the gene and protein expression levels of NOTCH1 and DLL4, and the down-regulation of miR-21-5p down-regulated the gene and protein expression levels of VEGFA and up-regulated the gene and protein expression levels of NOTCH1 and DLL4.

Our results demonstrated that the inhibition of the NOTCH1/DLL4 signaling pathway contributes to promoting angiogenesis, which is consistent with previous studies mentioned above. Meanwhile, our results also innovatively confirmed that overexpressing miR-21-5p in ADSC-derived exosomes inhibited the expression of NOTCH1 and DLL4 and activated the expression of VEGFA to promote angiogenesis. In addition, previous studies indicated that VEGFA induces the expression of NOTCH1 and DLL4 in endothelial cells, but overexpressing DLL4 in endothelial cells weakens VEGFA-induced cell proliferation and migration, suggesting that VEGFA is a positive regulator of DLL4 and DLL4 is a negative regulator of VEGFA [54, 55]. In the present study, the effects of miR-21-5p in ADSC-derived exosomes on DLL4 and VEGFA were the opposite. Therefore, we consider that VEGFA serves as the downstream regulator of DLL4 during the progression that miR-21-5p in ADSC-derived exosomes promotes angiogenesis. The above results indicated that miR-21-5p of ADSC-derived exosomes promoted angiogenesis by regulating the NOTCH1/DLL4/VEGFA signaling pathway. Although one previous study has demonstrated that ADSC-derived exosomal miR-21 promoted vascularization by up-regulating VEGF, this study further clarifies the essential role of ADSC-derived exosomal miR-21-5p in angiogenesis and the effects of miR-21-5p in promoting angiogenesis by regulating the NOTCH1/DLL4/VEGFA pathway [56].

So far, in this study, it was affirmed that the miR-21-5p of ADSC-derived exosomes promoted angiogenesis of EPCs to accelerate bone repair by targeting the NOTCH1/DLL4/VEGFA signaling pathway, providing a novel insight for the clinical treatment of bone defects. However, there are still some limitations in the present study. One limitation was that the effects of miR-21-5p of ADSC-derived exosomes in promoting angiogenesis to accelerate bone repair by regulating the NOTCH1/DLL4/VEGFA signaling pathway in vivo were not investigated. Therefore, the related investigation in vivo should

be conducted in the subsequent studies to sufficiently confirm the findings of this study. Another limitation was that the reason why the expression level of miR-21-5p in EPCs increased after co-culturing with ADSC-derived exosomes was not confirmed. We inferred that the increase in the expression level of miR-21-5p in EPCs might be attributed to the direct transfer from ADSC-derived exosomes because it was proved that the expression level of miR-21-5p in ADSC-derived exosomes was the highest in this study. However, the increase in the expression level of miR-21-5p in EPCs might be also attributed to the regulation of some long non-coding RNAs (lncRNAs) in exosomes or EPCs. The biomolecules contained in exosomes, especially for lncRNAs and miRNAs, play an essential role in intercellular communication, mediating multiple complex pathological processes of bone defects [57, 58]. Therefore, the effects of the lncRNA-miRNA-mRNA regulatory network mediated by ADSC-derived exosomes on EPCs could be further investigated in subsequent studies. In addition, it was reported that miR-21-5p also was one effective target in alleviating ferroptosis [59]. Meanwhile, the previous study indicated that ferroptosis and abnormal iron metabolism were the significant pathogenesis of osteoporosis [60]. Therefore, we believe that miR-21-5p is of great application value for the clinical treatment of multiple bone-related diseases, and its related mechanisms deserve further research.

Conclusion

Taken together, it was affirmed that the miR-21-5p of ADSC-derived exosomes promoted angiogenesis of EPCs to accelerate bone repair by targeting the NOTCH1/DLL4/VEGFA signaling pathway, providing a novel insight for the clinical treatment of bone defects.

Abbreviations

ADSCs	Adipose-derived stem cells
BMD	Bone mineral density
BV/TV	Percent bone volume
CCK-8	Cell counting kit-8
CD31	Platelet/endothelial cell adhesion molecule 1
CSBDs	Critical-sized bone defects
DLL4	Delta-like 4
EPCs	Endothelial progenitor cells
HA	Hyaluronic acid
H&E	Hematoxylin & eosin
IHC	Immunohistochemical
lncRNAs	Long non-coding RNAs
miRNAs	Micro RNAs
mRNAs	Messenger RNAs
NOTCH1	Neurogenic locus notch homolog protein 1
NTA	Nanoparticle tracking analysis
OCN	Osteocalcin
RUNX2	Runt-related transcription factor 2
Tb.N	Trabecular number
Tb.Th	Trabecular thickness
TEM	Transmission electron microscope
VEGFA	Vascular endothelial growth factor A

Acknowledgements

Not applicable.

Author contributions

H.Y. conceived and designed the study. L.C. wrote the manuscript and collected the relevant data. K.S. and R.Z. collected the relevant data and performed the statistical analyses. All the authors were aware of the group allocation at the different stages of the experiment, interpreted the data, and contributed to preparing this manuscript.

Funding

This work was supported by Science Foundation of Anhui Provincial Colleges and Universities (No. 2022AH050781) and Science Foundation of Anhui Medical Universities (No. 2023xkj063).

Availability of data and materials

The original data applied in this research are accessible from the corresponding author.

Declarations

Ethics approval and consent to participate

The project titled "Exosomes from adipose-derived stem cells accelerate bone repair by regulating endothelial progenitor cells to promote miR-21-5p-mediated angiogenesis" has been approved by the Fuyang Hospital Affiliated to Anhui Medical University on March 1, 2023, and in accordance with the guidelines of the Ethics Committee of Fuyang Hospital Affiliated to Anhui Medical University (ethical code: MDL2022-12–27-01).

Consent for publication

Not applicable.

Competing interests

All authors announce that there are no competing interests in publishing this article.

Author details

[1]Department of Orthopaedics, Fuyang Hospital of Anhui Medical University, Fuyang 236000, China. [2]Department of Intensive Care Unit, Fuyang Hospital of Anhui Medical University, Fuyang 236000, China.

Received: 1 September 2024 Accepted: 23 October 2024
Published online: 08 November 2024

References

1. Oh WT, Yang YS, Xie J, Ma H, Kim JM, Park KH, Oh DS, Park-Min KH, Greenblatt MB, Gao G. WNT-modulating gene silencers as a gene therapy for osteoporosis, bone fracture, and critical-sized bone defects. Mol Ther. 2023;31(2):435–53. https://doi.org/10.1016/j.ymthe.2022.09.018.
2. Sadowska JM, Ziminska M, Ferreira C, Matheson A, Balouch A, Bogle J, Wojda S, Redmond J, Elkashif A, Dunne N. Development of miR-26a-activated scaffold to promote healing of critical-sized bone defects through angiogenic and osteogenic mechanisms. Biomaterials. 2023;303:122398. https://doi.org/10.1016/j.biomaterials.2023.122398.
3. Storb R. Allogeneic bone marrow transplantation for aplastic anemia. Int J Hematol. 2024;119(3):220–30. https://doi.org/10.1007/s12185-022-03506-6.
4. Ciszyński M, Dominiak S, Dominiak M, Gedrange T, Hadzik J. Allogenic bone graft in dentistry: a review of current trends and developments. Int J Mol Sci. 2023. https://doi.org/10.3390/ijms242316598.
5. Heimes D, Pabst A, Becker P, Hartmann A, Kloss F, Tunkel J, Smeets R, Kämmerer PW. Comparison of morbidity-related parameters between autologous and allogeneic bone grafts for alveolar ridge augmentation from patients' perspective—a questionnaire-based cohort study. Clin Implant Dent Relat Res. 2024;26(1):170–82. https://doi.org/10.1111/cid.13242.

6. Huo L, Han Z, Jiao Z, Wei X, Xu Q, Ahmed A, Zheng J, Chen M, Yang C. Introduction of temporomandibular joint and skull base combined reconstruction by autogenous bone graft. Clin Oral Investig. 2023;27(6):2513–20. https://doi.org/10.1007/s00784-023-05065-4.
7. Guo T, Yuan X, Li X, Liu Y, Zhou J. Bone regeneration of mouse critical-sized calvarial defects with human mesenchymal stem cell sheets co-expressing BMP2 and VEGF. J Dent Sci. 2023;18(1):135–44. https://doi.org/10.1016/j.jds.2022.06.020.
8. Deng L, Hou M, Lv N, Zhou Q, Hua X, Hu X, Ge X, Zhu X, Xu Y, Yang H. Melatonin-encapsuled silk fibroin electrospun nanofibers promote vascularized bone regeneration through regulation of osteogenesis-angiogenesis coupling. Mater Today Bio. 2024;25:100985. https://doi.org/10.1016/j.mtbio.2024.100985.
9. Raftery RM, Gonzalez Vazquez AG, Walsh DP, Chen G, Laiva AL, Keogh MB, O'Brien FJ. Mobilizing endogenous progenitor cells using pSDF1α-activated scaffolds accelerates angiogenesis and bone repair in critical-sized bone defects. Adv Healthc Mater. 2024;13(23): e2401031. https://doi.org/10.1002/adhm.202401031.
10. Bixel MG, Sivaraj KK, Timmen M, Mohanakrishnan V, Aravamudhan A, Adams S, Koh BI, Jeong HW, Kruse K, Stange R. Angiogenesis is uncoupled from osteogenesis during calvarial bone regeneration. Nat Commun. 2024;15(1):4575. https://doi.org/10.1038/s41467-024-48579-5.
11. Arderiu G, Civit-Urgell A, Badimon L. Adipose-derived stem cells to treat ischemic diseases: the case of peripheral artery disease. Int J Mol Sci. 2023. https://doi.org/10.3390/ijms242316752.
12. Schneider I, Calcagni M, Buschmann J. Adipose-derived stem cells applied in skin diseases, wound healing and skin defects: a review. Cytotherapy. 2023;25(2):105–19. https://doi.org/10.1016/j.jcyt.2022.08.005.
13. Biniazan F, Stoian A, Haykal S. Adipose-derived stem cells: angiogenetic potential and utility in tissue engineering. Int J Mol Sci. 2024. https://doi.org/10.3390/ijms25042356.
14. Gečys D, Skredėnienė R, Gečytė E, Kazlauskas A, Balnytė I, Jekabsone A. Adipose tissue-derived stem cell extracellular vesicles suppress glioblastoma proliferation, invasiveness angiogenesis. Cells. 2023. https://doi.org/10.3390/cells12091247.
15. Singh S, Paul D, Nath VAR. Exosomes: current knowledge and future perspectives. Tissue Barriers. 2024;12(2):2232248. https://doi.org/10.1080/21688370.2023.2232248.
16. Zhang F, Jiang J, Qian H, Yan Y, Xu W. Exosomal circRNA: emerging insights into cancer progression and clinical application potential. J Hematol Oncol. 2023;16(1):67. https://doi.org/10.1186/s13045-023-01452-2.
17. Bhujel B, Oh SH, Kim CM, Yoon YJ, Kim YJ, Chung HS, Ye EA, Lee H, Kim JY. Mesenchymal stem cells and exosomes: a novel therapeutic approach for corneal diseases. Int J Mol Sci. 2023. https://doi.org/10.3390/ijms241310917.
18. Li S, Li Y, Zhu K, He W, Guo X, Wang T, Gong S, Zhu Z. Exosomes from mesenchymal stem cells: potential applications in wound healing. Life Sci. 2024;357:123066. https://doi.org/10.1016/j.lfs.2024.123066.
19. Zhang Y, Liu T. Adipose-derived stem cells exosome and its potential applications in autologous fat grafting. J Plast Reconstr Aesthet Surg. 2023;76:219–29. https://doi.org/10.1016/j.bjps.2022.10.050.
20. Shi X, Seidle KA, Simms KJ, Dong F, Chilian WM, Zhang P. Endothelial progenitor cells in the host defense response. Pharmacol Ther. 2023;241:108315. https://doi.org/10.1016/j.pharmthera.2022.108315.
21. Godbout C, Ryan G, Ramnaraign DJ, Hegner C, Desjardins S, Gagnon S, Bates BD, Whatley I, Schemitsch EH, Nauth A. Optimal delivery of endothelial progenitor cells in a rat model of critical-size bone defects. J Orthop Res. 2024;42(1):193–201. https://doi.org/10.1002/jor.25658.
22. Novak S, Tanigawa H, Singh V, Root SH, Schmidt TA, Hankenson KD, Kalajzic I. Endothelial to mesenchymal notch signaling regulates skeletal repair. JCI Insight. 2024. https://doi.org/10.1172/jci.insight.181073.
23. Gan F, Liu L, Zhou Q, Huang W, Huang X, Zhao X. Effects of adipose-derived stromal cells and endothelial progenitor cells on adipose transplant survival and angiogenesis. PLoS ONE. 2022;17(1): e0261498. https://doi.org/10.1371/journal.pone.0261498.
24. Huang H, Xu Z, Qi Y, Zhang W, Zhang C, Jiang M, Deng S, Wang H. Exosomes from SIRT1-overexpressing ADSCs restore cardiac function by improving angiogenic function of EPCs. Mol Ther Nucleic Acids. 2020;21:737–50. https://doi.org/10.1016/j.omtn.2020.07.007.
25. Li X, Xie X, Lian W, Shi R, Han S, Zhang H, Lu L, Li M. Exosomes from adipose-derived stem cells overexpressing Nrf2 accelerate cutaneous wound healing by promoting vascularization in a diabetic foot ulcer rat model. Exp Mol Med. 2018;50(4):1–14. https://doi.org/10.1038/s12276-018-0058-5.
26. Ying C, Wang R, Wang Z, Tao J, Yin W, Zhang J, Yi C, Qi X, Han D. BMSC-exosomes carry mutant HIF-1α for improving angiogenesis and osteogenesis in critical-sized calvarial defects. Front Bioeng Biotechnol. 2020;8:565561. https://doi.org/10.3389/fbioe.2020.565561.
27. Zhang Y, Xie Y, Hao Z, Zhou P, Wang P, Fang S, Li L, Xu S, Xia Y. Umbilical mesenchymal stem cell-derived exosome-encapsulated hydrogels accelerate bone repair by enhancing angiogenesis. ACS Appl Mater Interfaces. 2021;13(16):18472–87. https://doi.org/10.1021/acsami.0c22671.
28. Kashirina A, Yao Y, Liu Y, Leng J. Biopolymers as bone substitutes: a review. Biomater Sci. 2019;7(10):3961–83. https://doi.org/10.1039/c9bm00664h.
29. Zhang L, Jiao G, Ren S, Zhang X, Li C, Wu W, Wang H, Liu H, Zhou H, Chen Y. Exosomes from bone marrow mesenchymal stem cells enhance fracture healing through the promotion of osteogenesis and angiogenesis in a rat model of nonunion. Stem Cell Res Ther. 2020;11(1):38. https://doi.org/10.1186/s13287-020-1562-9.
30. Ren L, Zeng F, Deng J, Bai Y, Chen K, Chen L, Sun L. Inflammatory osteoclasts-derived exosomes promote bone formation by selectively transferring lncRNA LIOCE into osteoblasts to interact with and stabilize Osterix. Faseb j. 2022;36(2): e22115. https://doi.org/10.1096/fj.202101106RR.
31. Xiang X, Pathak JL, Wu W, Li J, Huang W, Wu Q, Xin M, Wu Y, Huang Y, Ge L. Human serum-derived exosomes modulate macrophage inflammation to promote VCAM1-mediated angiogenesis and bone regeneration. J Cell Mol Med. 2023;27(8):1131–43. https://doi.org/10.1111/jcmm.17727.
32. Fang S, Liu Z, Wu S, Chen X, You M, Li Y, Yang F, Zhang S, Lai Y, Liu P. Pro-angiognetic and pro-osteogenic effects of human umbilical cord mesenchymal stem cell-derived exosomal miR-21-5p in osteonecrosis of the femoral head. Cell Death Discov. 2022;8(1):226. https://doi.org/10.1038/s41420-022-00971-0.
33. Kong L, Wang Y, Wang H, Pan Q, Zuo R, Bai S, Zhang X, Lee WY, Kang Q, Li G. Conditioned media from endothelial progenitor cells cultured in simulated microgravity promote angiogenesis and bone fracture healing. Stem Cell Res Ther. 2021;12(1):47. https://doi.org/10.1186/s13287-020-02074-y.
34. Che D, Xiang X, Xie J, Chen Z, Bao Q, Cao D. Exosomes derived from adipose stem cells enhance angiogenesis in diabetic wound via miR-146a-5p/JAZF1 Axis. Stem Cell Rev Rep. 2024;20(4):1026–39. https://doi.org/10.1007/s12015-024-10685-8.
35. Dong L, Li X, Leng W, Guo Z, Cai T, Ji X, Xu C, Zhu Z, Lin J. Adipose stem cells in tissue regeneration and repair: From bench to bedside. Regen Ther. 2023;24:547–60. https://doi.org/10.1016/j.reth.2023.09.014.
36. Labusca L. Adipose tissue in bone regeneration - stem cell source and beyond. World J Stem Cells. 2022;14(6):372–92. https://doi.org/10.4252/wjsc.v14.i6.372.
37. Yu X, Odenthal M, Fries JW. Exosomes as miRNA carriers: formation-function-future. Int J Mol Sci. 2016. https://doi.org/10.3390/ijms17122028.
38. Liao Z, Chen Y, Duan C, Zhu K, Huang R, Zhao H, Hintze M, Pu Q, Yuan Z, Lv L. Cardiac telocytes inhibit cardiac microvascular endothelial cell apoptosis through exosomal miRNA-21-5p-targeted cdip1 silencing to improve angiogenesis following myocardial infarction. Theranostics. 2021;11(1):268–91. https://doi.org/10.7150/thno.47021.
39. Qiu S, Xie L, Lu C, Gu C, Xia Y, Lv J, Xuan Z, Fang L, Yang J, Zhang L. Gastric cancer-derived exosomal miR-519a-3p promotes liver metastasis by inducing intrahepatic M2-like macrophage-mediated angiogenesis. J Exp Clin Cancer Res. 2022;41(1):296. https://doi.org/10.1186/s13046-022-02499-8.
40. Qu Q, Liu L, Cui Y, Liu H, Yi J, Bing W, Liu C, Jiang D, Bi Y. miR-126-3p containing exosomes derived from human umbilical cord mesenchymal stem cells promote angiogenesis and attenuate ovarian granulosa cell apoptosis in a preclinical rat model of premature ovarian failure. Stem Cell Res Ther. 2022;13(1):352. https://doi.org/10.1186/s13287-022-03056-y.
41. Hu Y, Rao SS, Wang ZX, Cao J, Tan YJ, Luo J, Li HM, Zhang WS, Chen CY, Xie H. Exosomes from human umbilical cord blood accelerate cutaneous wound healing through miR-21-3p-mediated promotion of angiogenesis

and fibroblast function. Theranostics. 2018;8(1):169–84. https://doi.org/10.7150/thno.21234.
42. Ma J, Zhang Z, Wang Y, Shen H. Investigation of miR-126-3p loaded on adipose stem cell-derived exosomes for wound healing of full-thickness skin defects. Exp Dermatol. 2022;31(3):362–74. https://doi.org/10.1111/exd.14480.
43. Yang Y, Cai Y, Zhang Y, Liu J, Xu Z. Exosomes secreted by adipose-derived stem cells contribute to angiogenesis of brain microvascular endothelial cells following oxygen-glucose deprivation in vitro through microRNA-181b/TRPM7 axis. J Mol Neurosci. 2018;65(1):74–83. https://doi.org/10.1007/s12031-018-1071-9.
44. Vimalraj S. A concise review of VEGF, PDGF, FGF, Notch, angiopoietin, and HGF signalling in tumor angiogenesis with a focus on alternative approaches and future directions. Int J Biol Macromol. 2022;221:1428–38. https://doi.org/10.1016/j.ijbiomac.2022.09.129.
45. Gomez AH, Joshi S, Yang Y, Tune JD, Zhao MT, Yang H. Bioengineering systems for modulating notch signaling in cardiovascular development, disease, and regeneration. J Cardiovasc Dev Dis. 2021. https://doi.org/10.3390/jcdd8100125.
46. Cai Z, Zhao B, Deng Y, Shangguan S, Zhou F, Zhou W, Li X, Li Y, Chen G. Notch signaling in cerebrovascular diseases (review). Mol Med Rep. 2016;14(4):2883–98. https://doi.org/10.3892/mmr.2016.5641.
47. Ramasamy SK, Kusumbe AP, Wang L, Adams RH. Endothelial Notch activity promotes angiogenesis and osteogenesis in bone. Nature. 2014;507(7492):376–80. https://doi.org/10.1038/nature13146.
48. Zhang W, Han L, Wen Y, Su L, Li Y, Luo X. Electroacupuncture reverses endothelial cell death and promotes angiogenesis through the VEGF/Notch signaling pathway after focal cerebral ischemia-reperfusion injury. Brain Behav. 2023;13(3): e2912. https://doi.org/10.1002/brb3.2912.
49. Pitulescu ME, Schmidt I, Giaimo BD, Antoine T, Berkenfeld F, Ferrante F, Park H, Ehling M, Biljes D, Rocha SF. Dll4 and Notch signalling couples sprouting angiogenesis and artery formation. Nat Cell Biol. 2017;19(8):915–27. https://doi.org/10.1038/ncb3555.
50. Wu ZQ, Rowe RG, Lim KC, Lin Y, Willis A, Tang Y, Li XY, Nor JE, Maillard I, Weiss SJ. A Snail1/Notch1 signalling axis controls embryonic vascular development. Nat Commun. 2014;5:3998. https://doi.org/10.1038/ncomms4998.
51. Zhang Y, Zhang Y, Wang J, Gu H. Amarogentin inhibits liver cancer cell angiogenesis after insufficient radiofrequency ablation via affecting stemness and the p53-dependent VEGFA/Dll4/Notch1 pathway. Biomed Res Int. 2020;2020:5391058. https://doi.org/10.1155/2020/5391058.
52. Yi F, Xiao H, Song M, Huang L, Huang Q, Deng J, Yang H, Zheng L, Wang H, Gu W. BMSC-derived exosomal miR-148b-3p attenuates OGD/R-induced HMC3 cell activation by targeting DLL4 and Notch1. Neurosci Res. 2024;199:36–47. https://doi.org/10.1016/j.neures.2023.09.005.
53. Xiong Z, Hu Y, Jiang M, Liu B, Jin W, Chen H, Yang L, Han X. Hypoxic bone marrow mesenchymal stem cell exosomes promote angiogenesis and enhance endometrial injury repair through the miR-424–5p-mediated DLL4/Notch signaling pathway. PeerJ. 2024;12: e16953. https://doi.org/10.7717/peerj.16953.
54. Niderla-Bielińska J, Bartkowiak K, Ciszek B, Czajkowski E, Jankowska-Steifer E, Krejner A, Ratajska A. Pentoxifylline inhibits angiogenesis via decreasing Dll4 and Notch1 expression in mouse proepicardial explant cultures. Eur J Pharmacol. 2018;827:80–7. https://doi.org/10.1016/j.ejphar.2018.03.015.
55. Zhou R, Wang S, Wen H, Wang M, Wu M. The bispecific antibody HB-32, blockade of both VEGF and DLL4 shows potent anti-angiogenic activity in vitro and anti-tumor activity in breast cancer xenograft models. Exp Cell Res. 2019;380(2):141–8. https://doi.org/10.1016/j.yexcr.2019.04.025.
56. An Y, Zhao J, Nie F, Qin Z, Xue H, Wang G, Li D. Exosomes from adipose-derived stem cells (ADSCs) Overexpressing miR-21 promote vascularization of endothelial cells. Sci Rep. 2019;9(1):12861. https://doi.org/10.1038/s41598-019-49339-y.
57. Yang D, Chen Z, Xu Z, Qin L, Yi W, Long Y. Roles of stem cell exosomes and their microRNA carrier in bone and cartilage regeneration. Curr Stem Cell Res Ther. 2023;18(7):917–25. https://doi.org/10.2174/1574888x17666220817093305.
58. Ren YZ, Ding SS, Jiang YP, Wen H, Li T. Application of exosome-derived noncoding RNAs in bone regeneration: opportunities and challenges. World J Stem Cells. 2022;14(7):473–89. https://doi.org/10.4252/wjsc.v14.i7.473.
59. Hu Z, Li L, Li M, Zhang X, Zhang Y, Ran J, Li L. miR-21–5p inhibits ferroptosis in hepatocellular carcinoma cells by regulating the AKT/mTOR signaling pathway through MELK. J Immunol Res. 2023;2023:8929525. https://doi.org/10.1155/2023/8929525.
60. Bao J, Yan Y, Zuo D, Zhuo Z, Sun T, Lin H, Han Z, Zhao Z, Yu H. Iron metabolism and ferroptosis in diabetic bone loss: from mechanism to therapy. Front Nutr. 2023;10:1178573. https://doi.org/10.3389/fnut.2023.1178573.

Publisher's Note